

**Title:** High-throughput assessment of nanoparticle penetration of skin

**Authors:** Keana Scott

**Purpose:** In recent years, the number of products containing nano-sized materials has been increasing steadily because nanoparticles exhibit unique, size-dependent physical and chemical properties that are useful in pharmaceutical, cosmetics, and other industrial applications. However, these unique properties can have unexpected health and environmental effects. One of the major concerns over the widespread use of nanoparticles is the degree of nanoparticle absorption through skin. Although skin is a very effective barrier against most environmental contaminants, several studies have shown that nanoparticles can penetrate skin effectively when they are surface functionalized with charged moieties. When used as a topical drug delivery vehicle, such good skin penetrability is a desirable trait while the opposite is the case if nanoparticles are produced as industrial pollutants.

Proper assessment of nanoparticle penetration of skin requires evaluation of skin exposures to different nanoparticles in varying concentrations and environmental conditions. Currently there is no standard method to detect and quantify nanoparticle penetration of skin. Most evaluations of this type are carried out by individual companies, often resulting in incomplete and inconsistent data and analyses. Such inconsistency and heterogeneity in data make it difficult for regulatory agencies to make informed decision about the safety of nanoparticle based products.

NIST's expertise in method development, imaging, and microanalysis is being leveraged to develop efficient and accurate methods for detecting and quantifying nanoparticles in skin.

**Major Accomplishments:** A high throughput penetration study method was developed to address the time-dependent quality control issues and the difficulties in procuring sufficient skin samples for this type of multivariate experiments. This method allows dozens of experimental conditions to be tested simultaneously on a 70mm diameter piece of skin sample, see Figure 1. Preliminary experiments were performed on artificial skin samples where the samples were exposed to solutions of several types of quantum dots at several concentration levels. After 24 hours of incubation, the samples were fixed and processed for fluorescence and electron microscopy. The results from the preliminary analyses confirmed that multiple dosing conditions can be evaluated simultaneously without cross talk between the wells.

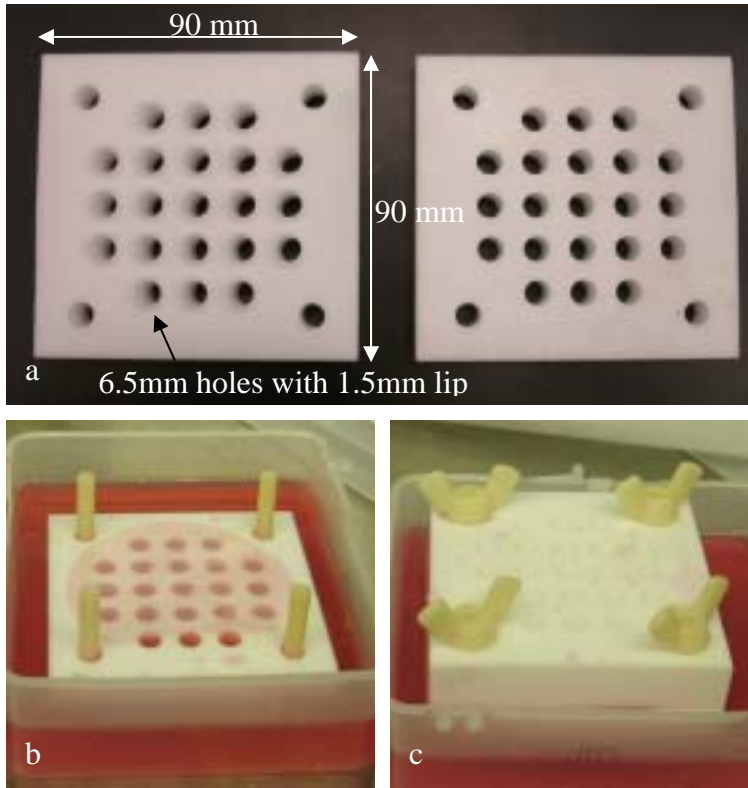


Figure 1: a) High-throughput diffusion plates, b) skin sample exposed to growth medium at the bottom, c) assembled plates

**Future Plans:** In addition to the optimization of the method and apparatus design to allow for multiple post processing options such as the use of different fixation methods or live cell stains, sample preparation and analysis techniques and methods for accumulated nanoparticle detection and quantification will be developed.

**Title:** Trace Detection Ion Mobility Spectrometry Analysis of Illicit Narcotics

**Authors:** Marcela C. Najarro, Rhyann Maditz, Abby Lindstrom (837.05),

**Purpose:** Ion mobility spectrometry (IMS) is a commonly used method for detecting and identifying volatile and semi-volatile organic compounds, principally in security and military venues. This technique is based on determining the drift velocities attained by gaseous ions, derived from sample molecules, in a weak electric field and at ambient pressure. The formation of ions from neutral sample molecules is necessary to determine ion mobility. Current national priorities in homeland security have led to an unprecedented level of utilization of trace explosive detection systems for counter-terrorism and law enforcement. At present, more than 50,000 handheld IMS analyzers have been distributed for chemical-weapons monitoring within the armed forces of several nations and more than 10,000 bench-top analyzers are used as explosives detectors in airports worldwide. Further advances in IMS technology have broadened its applications to the detection and identification of narcotics, human breath composition, and metabolites in bacteria. The use of IMS for trace detection of drugs has raised the intriguing possibility of using (simultaneously) the existing and widely deployed IMS explosives detection instruments for interdiction of narcotics and controlled substances. Such a capability may be of particular interest to US Customs and Border Patrol, the Drug Enforcement Agency (DEA), Federal Bureau of Investigations (FBI), the US Coast Guard and State and Local Law Enforcement. This work highlights the ongoing research aimed at determining the feasibility of using IMS for the rapid field identification of trace narcotics. The advantages of high sensitivity, high throughput, and low detection limits make this technique a promising approach for the trace detection of illegal narcotics.

**Major Accomplishment:** A series of practical experiments measured fingerprint IMS spectra as well as the linear dynamic range and detection limits of a series of illicit narcotics including cocaine, heroin, THC and methamphetamine. Typical detection limits for these compounds are in the range of 0.1-100 ng, which corresponds to the detection of a single particle with a diameter of a few micrometers. A multivariate parameter approach was used to determine optimal instrumental conditions for the different narcotics. Parameters explored include desorber temperature, drift/tube temperature, and inlet temperature. In order to confirm the target compound was correctly identified, a database of false positive alarms and interferences was developed resulting from a wide variety of over-the-counter medications, household and personal care products. Excipients and/or diluents commonly found in street narcotics were also carefully screened to determine their effect, if any, on IMS response. In addition, practical sampling issues were studied including optimal swiping procedures for best sensitivity as well as the influence of possible environmental background signatures that may be relevant to trace narcotics detection (for example, the widespread contamination of US currency by cocaine).

**Future Plans:** We intend to continue a series of experiments using additional IMS instruments in order to establish a recommended alarm threshold level for drugs, further optimize parameters for the detection of a particular drug of interest as well as characterize a list of potential sources of false positives.

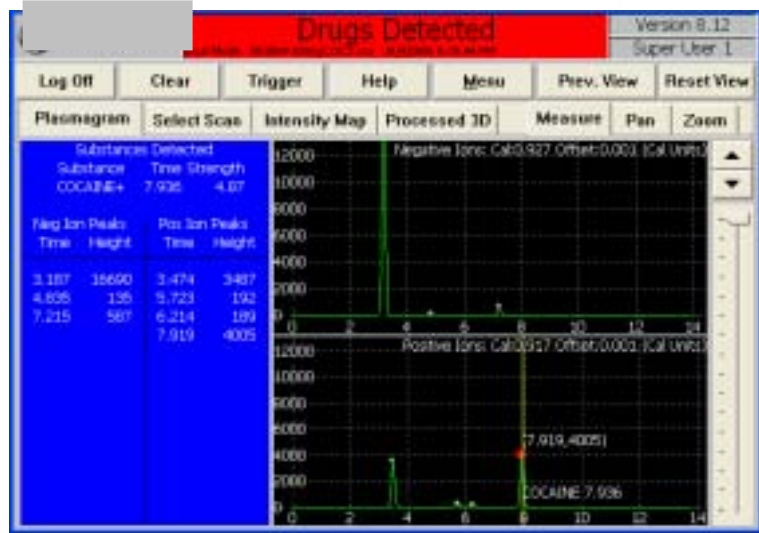


Figure 1. IMS response from a dual mode IMS system challenged with 100 ng of cocaine. Spectrum shows cocaine detection alarm on the positive ion channel.

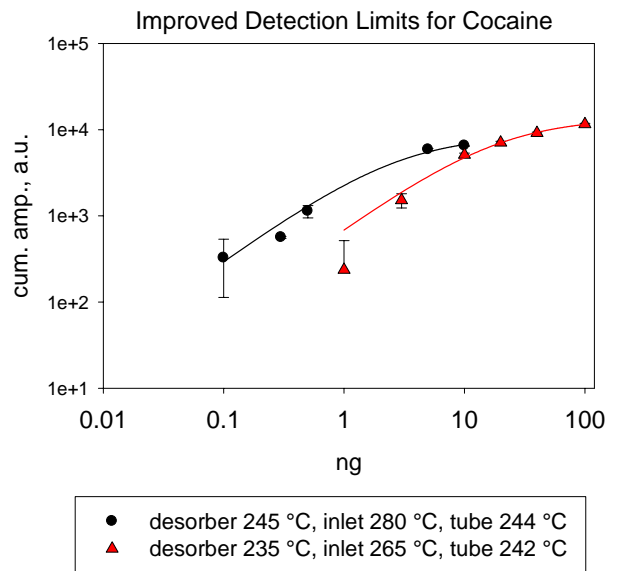
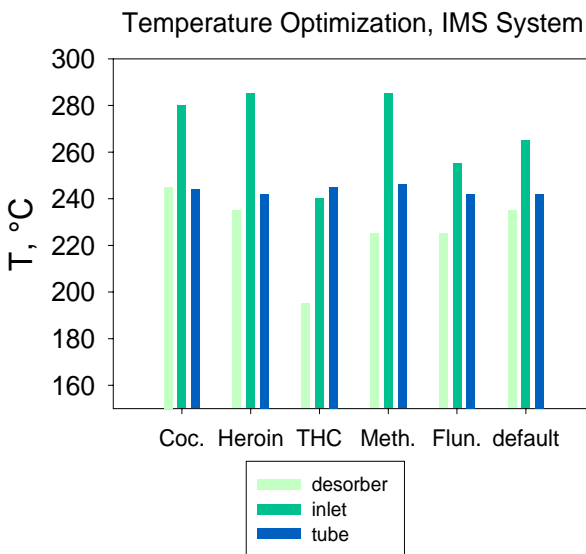


Figure 2(a). Optimal temperature settings for the desorber, inlet, and tube temperature for a commercial IMS system determined by noting optimal signal response for various illicit narcotics. Figure 2(b). Improved limit of detection for cocaine using optimized temperature settings.

## **Title: Automated Mapping of Explosives Particles in C-4 Fingerprints**

**Authors:** J.R. Verkouteren (837.05), J. Coleman (837.05) and Inho Cho (Transportation Security Laboratory)

**Purpose:** The detection of trace amounts of explosives at airports and other security venues is an important component of counterterrorism efforts. Currently, over 10,000 ion mobility spectrometry (IMS)-based explosive trace detectors (ETDs) are deployed at airports worldwide, in addition to the number used by the U.S. military and other federal agencies. A critical aspect of the deployment of ETDs is the calibration and testing of those instruments at the relevant threat levels. The fingerprint is considered one of the primary mechanisms for the transfer of trace amounts of explosives during bomb handling and preparation, and one of the target samples for collection. Critical properties that must be understood about these samples include the total mass and particle sizes of the explosives. The detection limits of ETDs are based on mass, but the collection of the sample is dependent on particle size.

To further the characterization of trace explosives samples, we have developed an automated polarized light microscopy (PLM) procedure for counting and sizing explosives particles in fingerprints made from C-4. We use both plane polarized light and crossed polarized light to produce complete images of the fingerprints, and also the size, shape, and locations of the RDX particles. A series of 50 prints were made at the Transportation Security Laboratory (TSL) from C-4, of which 36 were characterized to determine particle size distributions of the RDX particles. For selected fingerprints, the mass of RDX was determined by two techniques, particle counting and GC  $\mu$ -ECD (gas chromatography electron capture detection) analysis. The developed methodology can be used to rapidly characterize C-4 fingerprints with relatively little operator input, so that a large number of samples can be evaluated. This will aid in the development of “threat libraries” which can serve to delineate the performance requirements for ETDs. In addition, the analysis is nondestructive and the samples can be used after characterization as test materials for ETDs.

**Major Accomplishment(s)** – A series of 50 C-4 fingerprints were characterized, and the results show that the transfer of material through fingerprints is quite variable. This suggests that standard test materials cannot be developed simply by controlling the preparation of the fingerprints, and that a method is required for non-destructive analysis after fingerprint generation. Using our PLM method, the particle size distributions and the particle heights measured in the fingerprints can be used to estimate the mass of RDX in the fingerprint. These estimates of mass were found to be generally within  $\pm 60$  % relative of the results obtained from GC  $\mu$ -ECD, which is quite encouraging for a particle counting approach. Our data suggest that the particle diameters to target for improved ETD performance range from 10  $\mu$ m to 20  $\mu$ m. These particle sizes are found in sufficient abundance throughout the series of 50 prints, and have sufficient mass for detection purposes.

**Impact** – These results provide critical information for testing and improving the performance of ETDs, specifically in the development of appropriate test materials. ETD manufacturers and agencies responsible for the deployment of the equipment are specifically requesting this type of information. Our own efforts to develop test materials are guided by the knowledge of the characteristics of the real samples.

**Future Plans** – This activity will continue in order to characterize additional explosive threats (using a list of threats developed by the TSL). We plan to add capability to the method by using a polarized light microscope outfitted with FT-IR detection.

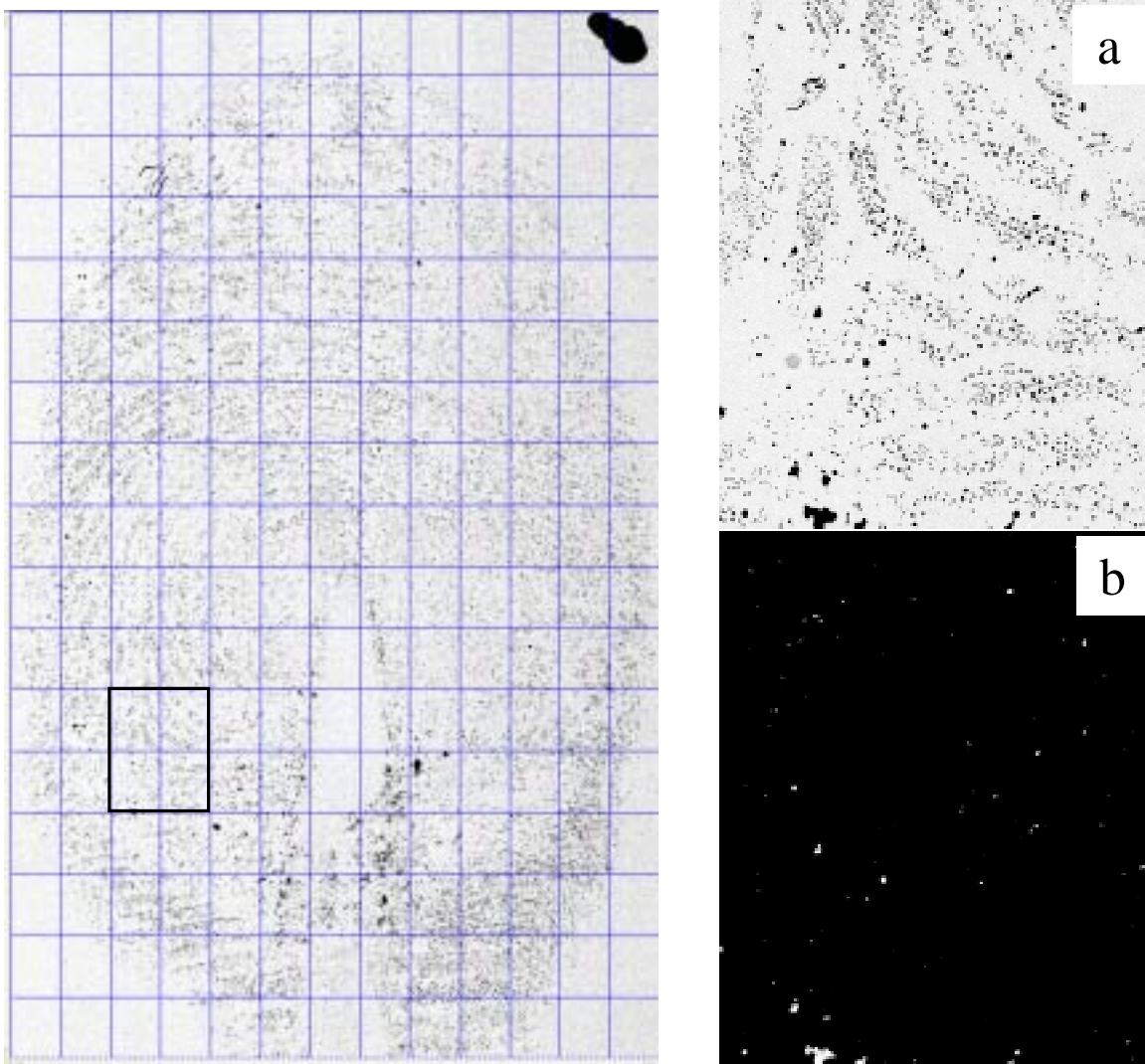


**Figure 1.** Plane polarized light image of visible fingerprint on left with overlay of grid pattern showing sizes of individual tiles used to collect the image. Selected area marked by bold box is shown in plane polarized light in (a) and crossed polarized light in (b). RDX particles are the birefringent (bright) particles observed in the crossed polarized light image.

**Title:** Infrared Microscopy with a ZnSe Solid Immersion Lens

**Author:** C.A. Michaels

**Purpose:** Nondestructive analysis of the chemical composition of materials on microscopic length scales requires a spectroscopic technique with high spatial resolution, sensitivity sufficient to analyze small amounts of material, and chemical specificity. Infrared (IR) spectral microscopy is such a technique, exploiting the chemical specificity of infrared absorbance spectroscopy to allow the spatial mapping of chemical constituents of heterogeneous materials. This technique finds application in a wide variety of industry sectors, including chemicals, pharmaceuticals, forensics, and microelectronics. The rapid pace of device miniaturization in these and other sectors drives the need for chemical imaging techniques with spatial resolution relevant to the critical dimensions of the device or material. The attainable spatial resolution in conventional IR microscopes is limited to values in the 20-30 micrometer range. Although this resolution is suitable for a broad class of analytical problems, it is nearly two orders of magnitude worse than that of the best visible light microscopy. Improvements in the spatial resolution of this technique would extend its considerable power to a significant set of advanced materials analysis challenges for which the current resolution is insufficient. Solid immersion lens (SIL) imaging involves the use of a lens (usually hemispherical) made from a material with a high index of refraction,  $n$ . Converging light impinging on the curved surface of the hemisphere forms an aberration free focus at the center of the bottom surface of the lens, yielding an increase in resolution by a factor of  $n$ . This improvement can be quite significant, particularly in the IR, where commonly used materials (*e.g.*, ZnSe, Ge) have indices in the range 2 to 4. This technique has been widely explored in the visible spectral region for optical data storage but little effort has been directed toward its use for chemical imaging with IR light. Application of SILs to IR microscopy offers the possibility of extending the spatial resolution of this technique and its utility in the analysis of advanced materials. Development and validation of next-generation measurement techniques, such as high spatial resolution IR SIL microscopy, benefits industrial and government customers, in alignment with the NIST mission.

**Major Accomplishments:** A reflection mode, imaging IR microscope incorporating a ZnSe hemispherical SIL has been constructed and its imaging performance validated. Key components of the microscope include a broadband ( $\sim 200\text{ cm}^{-1}$ ) IR laser source, an Indium Antimonide (InSb) focal plane array detector and a 0.65 numerical aperture, reflective Schwarzschild objective. The performance of the microscope was characterized by imaging  $2.5\text{ }\mu\text{m}$  diameter polystyrene (PS) beads dispersed on both a gold film (no SIL), and the bottom surface of the SIL. Figure 1(a) is a  $(95\pm 1) \times (95\pm 1)\text{ }\mu\text{m}$  reflection image of the PS beads on gold imaged without the SIL at a wavelength  $\lambda = 3.4\text{ }\mu\text{m}$ . The PS spheres scatter light out of the collection cone of the objective and thus appear dark compared to the reflective gold. Figure 1(b) is a  $(36\pm 1) \times (36\pm 1)\text{ }\mu\text{m}$  reflection image of the PS beads deposited on the bottom surface of the ZnSe SIL, also at a wavelength  $\lambda = 3.4\text{ }\mu\text{m}$ . Variation in the degree of total internal reflection (TIR) is the dominant contrast mechanism in this image. Most of the light in the angular range collected by the objective undergoes TIR at the ZnSe/air interface while propagating at the ZnSe/PS interface. Thus the PS spheres appear dark as the propagating light does not reach the reflection path detector. Figure 2 shows x-axis cross sections through the PS spheres circled in Fig. 1, allowing a comparison of the apparent sphere sizes. The FWHM of the sphere feature in the air image (1(a)) is approximately  $5.3\text{ }\mu\text{m}$ , reflecting some convolution of the microscope point spread function (PSF) with the actual

PS sphere size. The FWHM of the sphere in the SIL image (1(b)) is approximately  $3.2\ \mu\text{m}$ , demonstrating the increased resolving power of the SIL microscope. Using a simple model of the PSF, the resolution with the SIL can be shown to increase by a factor of 2.3 over the value in air, in good agreement with the expected value of 2.43 ( $n_{\text{ZnSe}}$ ). This comparison of air and SIL images demonstrates that IR imaging with off-the-shelf ZnSe hemispheres as immersion lenses is a straightforward approach to increasing the attainable spatial resolution in IR microscopy.

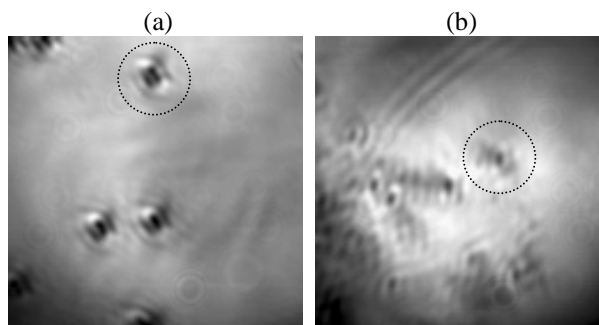


**Figure 1.** (a)  $(95\pm 1) \times (95\pm 1)\ \mu\text{m}$  reflection image of  $2.5\ \mu\text{m}$  PS spheres deposited onto a gold coated microscope slide acquired at  $\lambda = 3.4\ \mu\text{m}$ . (b)  $(36\pm 1) \times (36\pm 1)\ \mu\text{m}$  SIL image of  $2.5\ \mu\text{m}$  PS spheres deposited onto the flat surface of the 2 mm diameter ZnSe hemispherical SIL, acquired at  $\lambda = 3.4\ \mu\text{m}$ .

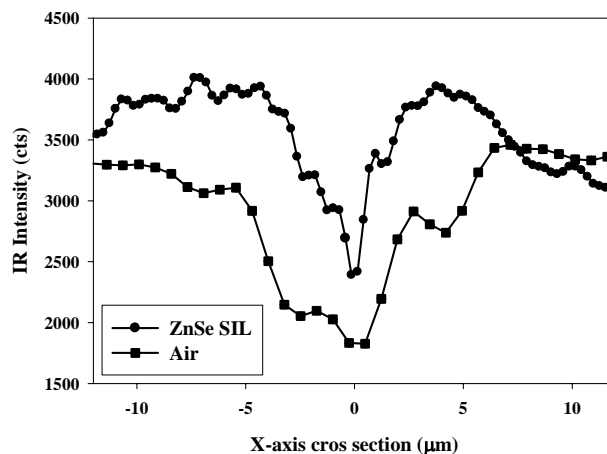


**Figure 2.** X-axis cross sections through PS spheres circled in air image (Fig. 1(a), squares) and ZnSe SIL image (Fig. 1(b), circles).

**Future Plans:** Acquisition of spectral images that contain the desired chemical contrast is a critical milestone for this project. A method for incorporating wavelength dispersion (e.g., FT interferometer) is currently being implemented to address this issue. Additionally, the construction of a transmission path microscope is underway. This version will incorporate a bimorph actuator for fine control over the sample/lens distance.

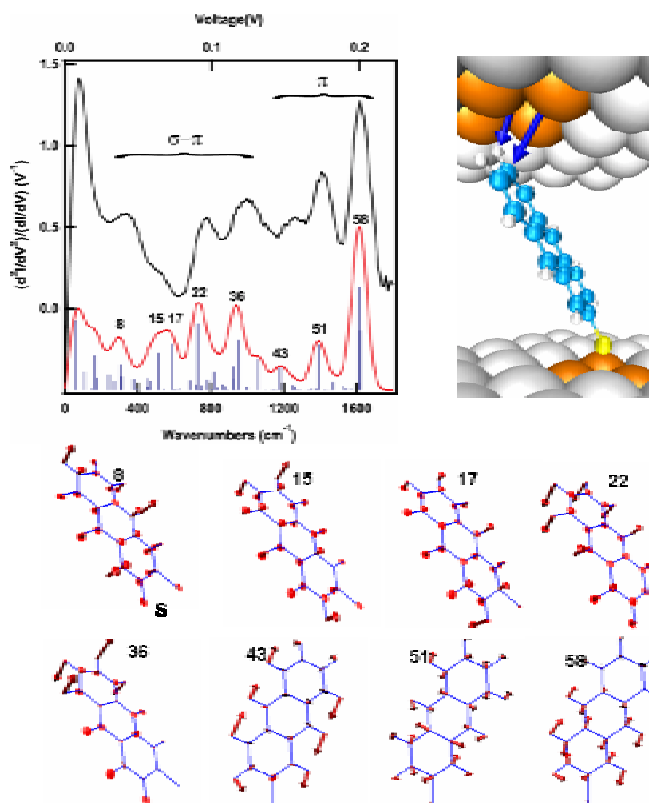
**Pubs/Outputs:** A manuscript describing this work has been completed and will be submitted to Applied Physics Letters. This work has also been presented in invited talks at the Eastern Analytical Symposium, Dow Chemical and the Federation of Analytical Chemistry and Spectroscopy Societies (FACSS) national meeting.

## Title: Tracing Electronic Pathways in Molecules Using Inelastic Electron Tunneling Spectroscopy

**Authors:** J.G. Kushmerick, J.M. Beebe (*Div. 836*), R.D. van Zee (*Div. 836*), D.R. Stewart (*Hewlett-Packard Laboratories*), A. Troisi (*University of Warwick*) and M.A. Ratner (*Northwestern University*)

**Purpose:** *Molecular Electronics* envisions that the nonlinear characteristics of individual or small ensembles of molecules will provide the active element in future electronic devices enabling some of the high-cost semiconductor fabrication processes to be replaced by low-cost chemical synthetic methods. A detailed understanding of charge transport across metal-molecule-metal junctions, the fundamental building block of a molecular electronic device, is paramount for molecular electronics to transition from a research endeavor into a viable technology. Our efforts have focused on the fundamental physical measurements which will provide the needed insight to enable the rational design of molecular electronic devices.

**Major Accomplishments:** Using inelastic electron tunneling spectroscopy (IETS) to measure the vibronic structure of non-equilibrium molecular transport, aided by a quantitative interpretation scheme based on non-equilibrium Greens function/density functional theory methods, we are able to characterize the actual pathways that electrons traverse when moving through a molecule in a molecular transport junction. The pathways idea has been present in physical organic chemistry for years in connection with reaction mechanisms, and has been widely used in the interpretation of electron tunneling pathways in proteins, but no distinct observations have been made. We show that the IET spectra directly index electron tunneling pathways along the given normal coordinates of the molecule. One can then interpret the maxima in the IETS spectrum in terms of the specific paths that the electrons follow, as they traverse the molecular junction. IETS measurements therefore not only prove (by the appearance of molecular vibrational frequencies in the spectrum) that the tunneling charges in fact pass through the molecule, but also can be used to determine just what the transport pathways are, and how they change with the geometry and placement of molecules in junctions.



Experimental (black) and computed spectra (red) of an anthracene thiol junction. The observed normal modes belong to two groups: out of plane modes that favor the intercommunication between the  $\sigma$  and  $\pi$  tunneling channels and in plane C-C stretches that modulate the main  $\pi$ -type tunneling channel. The molecules couple to the electrode via the  $s$  orbital of the hydrogen and the  $p_z$  orbital of the carbon.

**Future Plans:** We plan to use this strong coupling of inelastic electron tunneling spectroscopy and quantitative interpretation scheme to determine the pathways for charge transport in molecules with more complex chemical and electronic structures. The over riding goal is that through detailed understanding of the fundamental processes in charge transport across molecular junctions rational design of molecular devices will become a reality.

**Pubs/Outputs:** A manuscript describing these findings has been completed and will submitted for publication, and these results have been disseminated to the Defense Advanced Research Projects Agency, which provided partial funding for this research.

## Title: Charge Transport in Molecular Thin Films on Oxide and Metallic Surfaces

**Authors:** L.C. Teague, J.G. Kushmerick, S.K. Cotts (College of William and Mary), and W.R. Kwochka (Western Carolina University)

**Purpose:** This project focuses on experimental and theoretical investigations of the structure and charge transport characteristics of thin films of organic pi systems chemically bound to oxide and metallic surfaces. The structure and molecular organization within the films has a large impact on the through film charge transport. This project is of interest for the molecular and organic electronics efforts within CSTL, MSEL and EEEL.

**Major Accomplishments:** Vapor deposition is commonly used to form multilayers of organics that can serve as active elements in device structures. The molecular structure within these as-deposited films is closely related to the bulk crystal structure of the molecules. This bulk crystal structure usually consists of a herringbone type arrangement of the molecules, which has been shown, theoretically, to have a large impact on the charge transport in organic and molecular based devices. New methods for solution phase deposition and optimization of charge transport of active organic/molecular layers is of interest for more efficient devices.

In our approach, solution phase chemical methods are used to tether the active molecules to the surface to form ordered monolayer films of charge transport moieties. Our initial theoretical simulations of these types of structures reveal their potential as active layers in monolayer organic devices. These studies predict that better molecular overlap can be achieved by chemically binding the pi systems to the surface via an alkyl linker (Figure 1). By anchoring the molecules to the surface, the herringbone structure of the bulk crystals is not predicted and the calculated charge transport (mobility) within well-ordered films is comparable to that of vapor deposited systems as reported in the

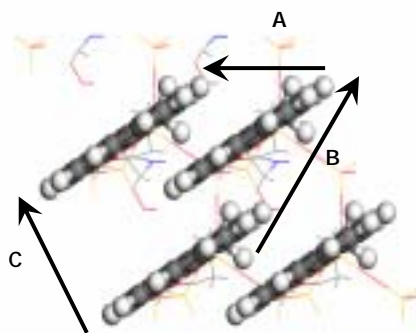
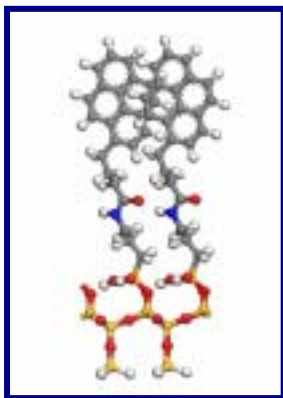
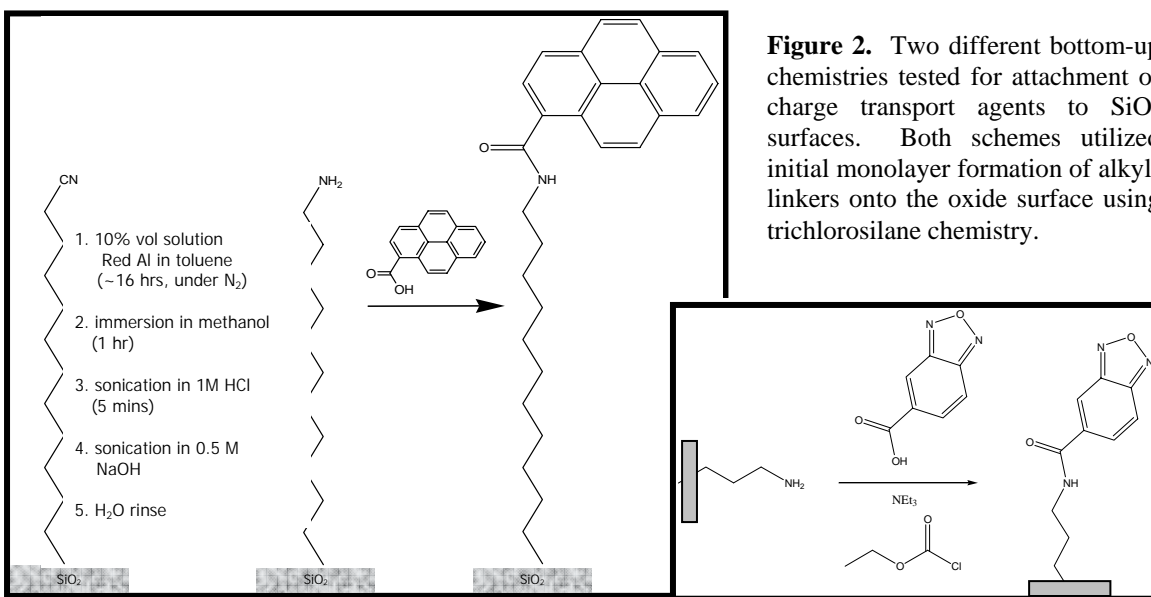


**Figure 1.** Side-on (left) and top-down view (right) of pyrene film attached to SiO<sub>2</sub> surface via alkyl linker. Hole mobilities were calculated for each nearest neighbor interaction and are listed in text.

literature. Charge mobilities were calculated for each of the nearest-neighbor interactions in the films of pyrene (hole transport agent) and 2,1,3-benzoxadiazole-5-carboxylic acid (electron transport agent) tethered to the SiO<sub>2</sub> surface. For pyrene (Figure 1), the calculated hole mobilities (A= 12.869 cm<sup>2</sup>/V·s ; B= 9.299 cm<sup>2</sup>/V·s; C= 0.138 cm<sup>2</sup>/V·s) show that the most efficient charge transport in the pyrene film is in the direction of A.

While theoretical investigations of these films show their promise for creating efficient devices at the monolayer level, experimental studies show the challenges of making such films a reality. In our studies, a number of bottom-up chemical assembly methods were explored to create monolayers of charge transport agents tethered to the SiO<sub>2</sub> surface (Figure 2). Film formation was characterized using AFM, FTIR, contact angle and ellipsometric techniques. Following optimization of these attachment techniques, films were incorporated into field effect transistor device structures for analysis of their charge transport characteristics. These devices were created using photolithographic methods and did not show transistor characteristics. We believe that these results are related to two different factors including: (1) the size (channel length and width) of devices made using photolithographic techniques and (2) the irreproducibility of monolayer films of the initial silane linkers.



**Future Plans:** A combination of FTIR, ellipsometry, contact angle, and STM techniques will be used to determine the influence of alkyl linker chain length on monolayer film formation and order on both Au and SiO<sub>2</sub> surfaces. We will further evaluate what influence ordering within these films may have on solution phase deposition of additional molecular layers. Theoretical simulations will be expanded to include a variety of charge transport agents tethered to the SiO<sub>2</sub> surface. A comparison of these systems will show the influence of the film structure on the through-film charge transport and will be used as a comparison to the charge transport characteristics of bulk systems presented in the literature.

## **Title: Structural contribution to Charge Transport across Ni-Octanedithiol Multilayer Junctions**

**Authors:** L.H. Yu, C. D. Zangmeister (*Div. 836*) and J.G. Kushmerick

**Purpose:** Molecular-based electronics have the potential to become a complementary or even the replacement technology for the semiconductor-based electronics we use today. The ability to identify reliably the origin of the electrical transport characteristics of any given molecular-based device is one of the critical technical goals that many in the field are endeavoring to meet. We are focused on applying an electronically based spectroscopic technique on novel molecular systems to gain fundamental understanding to the functional mechanism for molecular electronic devices.

**Major Accomplishments:** We demonstrate that the transport characteristics of a molecular junction can be directly influenced by the active design of the molecular components. Using 1,8-octanedithiol (**C8**) and Ni(II) ions as the molecular building blocks, we employ a bottom-up approach to assemble molecular multilayer structures, which exhibit electrical transport behavior commensurate with their structural design. The structures of the multilayers, were determined by ellipsometry, Fourier transform infrared spectroscopy and X-ray photoelectron spectroscopy. A schematic of the resultant multilayer is given in Fig. 1.

The electrical transport measurements of these molecular devices were performed with a custom-built cryogenic cross-wire tunneling junction apparatus, and the vibrational modes of the multilayer were measured electronically by the inelastic electronic tunneling (IET) spectroscopy. In these molecular devices we observe vibrational excitations that match the known and calculated vibrational spectra of the molecular multilayer. Fig. 1 shows the IET spectra of **C8** monolayer and **C8**/Ni(II) multilayer, along with mode/vibrational assignments. A number of these devices also exhibit stochastic gating due to time varying charging of defects in the molecular multilayer. We show that the electrical transport through these molecular multilayer junctions is dominated by the intrinsic properties of the multilayer.

**Future Plans:** We plan to investigate the magnetic and magnetoresistive properties of these multilayer structures. One goal of this project is to understand how an external magnetic field can influence the electrical transport behavior of a molecular device that is incorporated with ferromagnetic ions.

**Output:** A manuscript describing this work has been published: L.H. Yu, C.D. Zangmeister and J.G. Kushmerick, "Structural Contributions to Charge Transport across Ni-Octanedithiol Multilayer Junctions", *Nano Letters* **6**, 2515-2519 (2006).

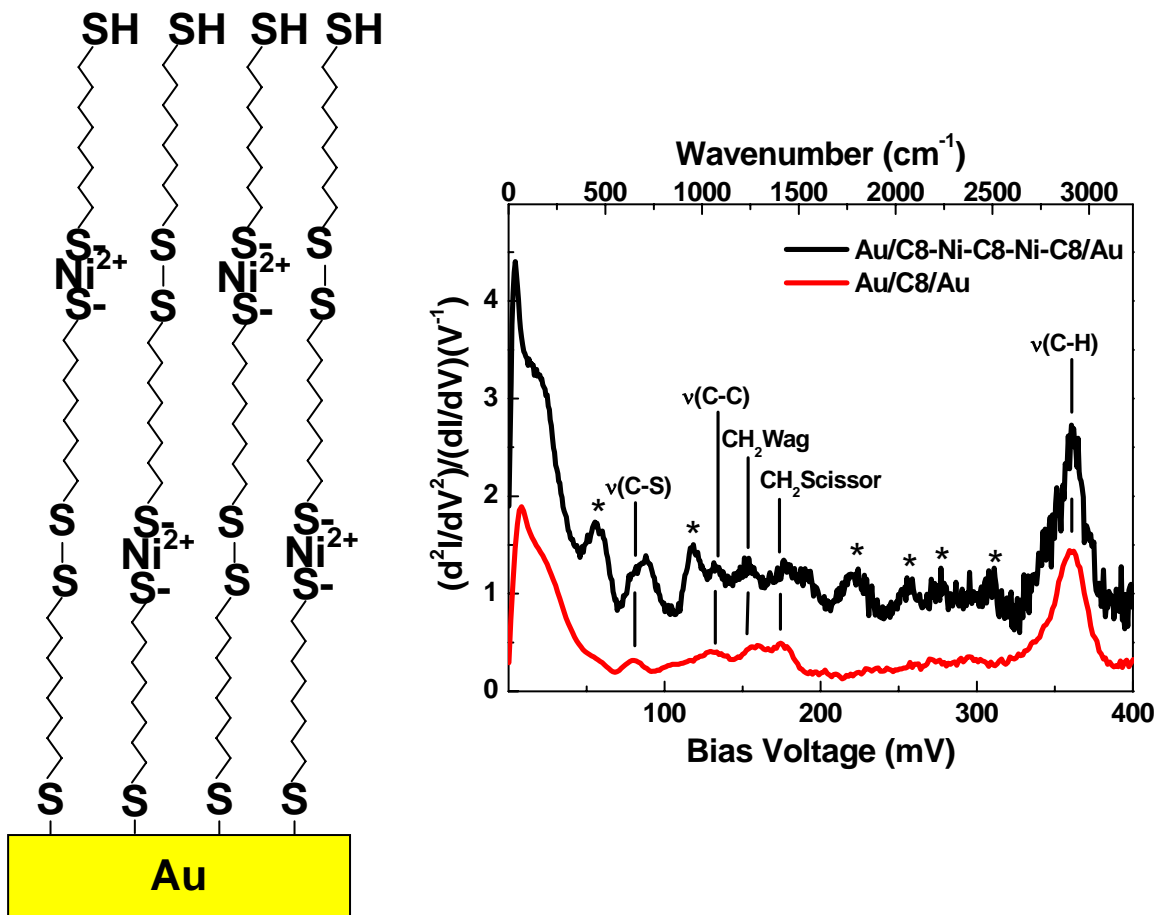


Fig. 1: (Left) Schematic structure of C8/Ni(II) multilayer. (Right) Inelastic electron tunneling spectra of a C8-Ni-C8-Ni-C8 multilayer junction (black) and a C8 monolayer junction (red). The black trace is shifted vertically by  $0.5 V^{-1}$  for clarity. Mode assignments are from comparison to previous experimental results and density functional theory calculations. The asterisks mark the IETS mode observed only in the molecular multilayer junction.

## **Title: Broadband Coherent anti-Stokes Raman Spectroscopy Characterization of Polymer Thin Films**

**Authors:** Z.D. Schultz, M.C. Gurau and L.J. Richter

**Purpose:** The advent of robust, ultrafast lasers has enabled the application of coherent nonlinear spectroscopies to routine sample characterization. Coherent anti-Stokes Raman scattering, CARS, is the nonlinear equivalent of conventional spontaneous Raman scattering. Conventional Raman is a scattering process, and the signal is highly dependent upon collection efficiency. The coherent nature of the CARS process gives rise to a directional signal simplifying collection and improving the sensitivity. Surprisingly, there has been little work exploring the utility of CARS as a thin film diagnostic. Surface enhanced Raman scattering, SERS, has been used to probe the interfacial region of thin polymer films on metal surfaces. However, limitations inherent in SERS leave much unknown. For example, SERS enhancement often requires roughened coinage metal (Au, Ag, Cu) substrates. It is difficult to characterize film surface interactions when enhancement only comes from particular surface sites. Additionally, SERS enhancement only extends a few nm into the film, making it sensitive to the interface, but blind to contributions from further into the bulk. CARS alleviates both of these restrictive conditions as nonlinear mixing occurs throughout the focal overlap region of the incident beams and is not dependent upon substrate enhancement. We have demonstrated a simple modification to an existing nonlinear spectrometer that enables CARS characterization of thin polymeric films. We find that this methodology permits rapid acquisition of high signal-to-noise (S/N) spectra. Indeed, broad-bandwidth CARS spectroscopy has been demonstrated to have clear sensitivity advantages over conventional Raman spectroscopy for the characterization of thin films. The spectroscopy shows special promise for the characterization of the ultrathin organic films required for advanced electronic applications such as organic light emitting diodes and thin film transistors.

**Major Accomplishments:** A schematic of a typical, degenerate CARS experiment is given in Figure 1. Two laser pulses are incident on the sample, with frequencies  $\nu_1$  and  $\nu_2$ . They mix nonlinearly to give an output pulse at the frequency  $\nu_3=2\nu_1-\nu_2$ . If the difference frequency  $\delta=\nu_1-\nu_2$  is resonant with a Raman active transition in the sample, the mixing process is enhanced and a vibrational spectrum can be recorded. In the NIST experiments, a 100 fs pulse duration laser is used to generate a broadband packet of frequencies at  $\nu_2$ ; this provides high peak fields, improving the nonlinear mixing, and simplifies the data collection by reducing the need to tune the laser providing  $\nu_2$ .

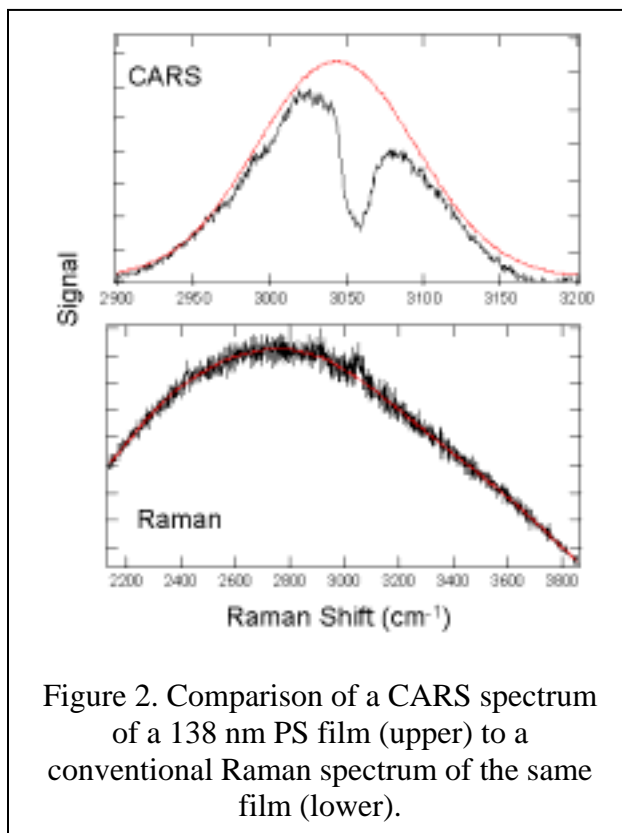
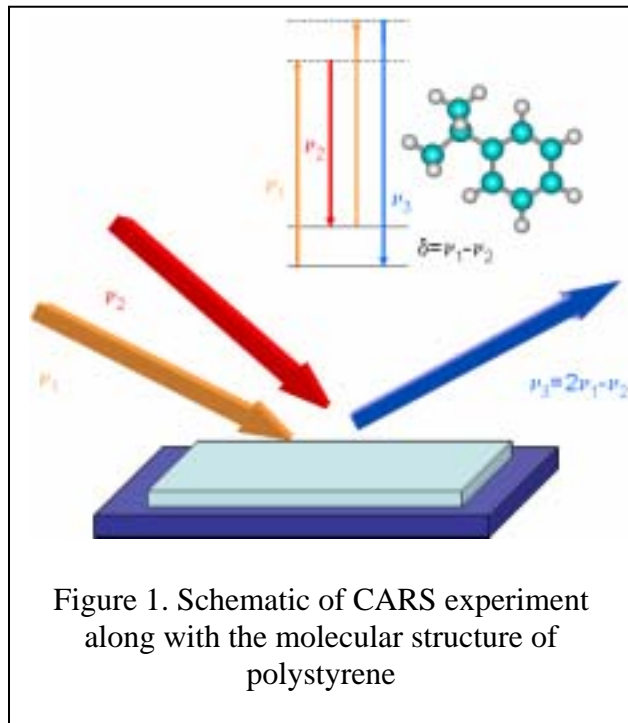
Experiments were performed with a variety of thin polymer film samples to establish the potential of broad-bandwidth CARS in comparison with conventional Raman spectroscopy. Shown in the lower panel of Figure 2 is the Raman spectrum of a 138 nm polystyrene, - $[\text{CH}_2\text{CHC}_6\text{H}_5]_n$ -, film, recorded with a 633 nm laser and a commercial Raman collection system. The weak feature at  $3060\text{ cm}^{-1}$  is the Raman active fully symmetric stretching vibration of the 5 C-H bonds on the phenyl ring ( $\text{C}_6\text{H}_5$ ; see schematic in Fig. 1). The broad background is due to fluorescence from both the polymer and the Si substrate. Shown in the upper panel of Figure 2 is the CARS spectrum of the same film. For the CARS measurement, the polystyrene (PS) vibrational features appear as ‘anti resonances’ on a non-resonant background. Both the conventional and CARS spectra in Figure 1 were taken with identical acquisition times (60 s)

and comparable total power onto the sample. The CARS spectrum is clearly of much higher quality. Quantitative analysis of the data indicates that CARS measurement displays a  $\sim x25$  improvement in the S/N.

Additional experiments for films of various polymers have been performed on diverse substrates (Si, Au, glass). The film thickness was varied from  $\sim 20$  nm to  $\sim 300$  nm. In all cases, high quality vibrational spectra were acquired, with demonstrated improved S/N compared to conventional Raman spectra. A mathematical framework for the quantitation of the CARS spectra, accounting for the influence of the substrate dielectric response, was developed and shown to be consistent with the measurements.

**Future Plans:** In addition to providing chemical structure information, via the vibrational spectrum, the CARS scattering process is exquisitely sensitive to both the symmetry and orientation of the sample. Standard procedures to quantify these aspects of the sample, via detailed polarization studies, will be developed and verified.

**Publications** – Z.D. Schultz, M.C. Gurau and L.J. Richter, *Broadband Coherent anti-Stokes Raman Spectroscopy Characterization of Polymer Thin Films*, Appl. Spec. **60**, 1097 (2006).



**Title: Study of the Potential Dependence of Co-Adsorption of PEG, Cl<sup>-</sup>, and SPS/MPS on Cu using *In-Situ* Spectroscopic Ellipsometry**

**Authors:** M.L. Walker, L.J. Richter and T.P. Moffat (Div. 855)

**Purpose:** Cu is the current material of choice for interconnects in integrated circuit (IC) chips ubiquitously used as components in modern day technology. Electrodeposition is the method in which Cu is plated into sub-micrometer structures such as trenches and vias, forming the electrical interconnections between the millions of transistors contained on an IC. This plating process is controlled by specific additives in the electrochemical bath such as polyethylene glycol, Cl<sup>-</sup> ion, and either 3-mercaptopropyl sulfonate (MPS) or bis-3 sulfopropyl disulfide (SPS). These additives adsorb onto the surfaces of trenches and vias in a particular sequence, facilitating defect-free Cu filling of these sub-micrometer structures; this process is called superconformal filling. As device feature sizes shrink, a greater understanding of the interactions of the additives in the baths as a function of potential must be realized in order formulate baths with greater dynamic range to achieve superconformal filling in vias and trenches with smaller dimension and correspondingly higher aspect ratios. Research of this type is important to the microelectronics industry in the effort to achieve the technology nodes of 65 nm and lower.

**Major Accomplishments:** In-situ spectroscopic ellipsometry (SE) has been used successfully to characterize additive adsorption onto sample substrates. Initial work focused on the co-adsorption of polyethylene glycol (PEG) and Cl<sup>-</sup> ion onto the coinage metals Cu, Ag and Au in the absence of Cu plating salts at a potential relevant to electroplating,  $-0.65 V_{MSE}$ . It was determined that PEG adsorbed onto the metal substrates in the presence of Cl<sup>-</sup> ion as a layer of approximately 0.6 nm thick; in the absence of Cl<sup>-</sup>, PEG adsorption was minimal. These two components form the inhibitory layer on the substrate, capable of hindering Cu deposition under true plating conditions. SPS and MPS, “catalysts” or “accelerants”, adsorb slower than PEG/Cl<sup>-</sup> but upon adsorption serve to lift the inhibition caused by PEG/Cl<sup>-</sup> and thus “accelerate” plating with respect to this layer. This is demonstrated in Fig. 1 in which Cl<sup>-</sup> and PEG are added, followed the addition of MPS. The growth of the model thickness curve subsequent to MPS addition is the action of MPS on the substrate in conjunction with the PEG/Cl<sup>-</sup> layer. The disruption of the PEG/Cl<sup>-</sup> layer is seen upon a significant reduction in the concentration of additives in the bath by a back dilution process; the more stable thiol remains adsorbed to the substrate.

The potential dependence of additive interactions was examined at the potentials of  $-0.65 V_{MSE}$ ,  $-0.75 V_{MSE}$ , and  $-0.85 V_{MSE}$ , industrially relevant plating potentials. In Fig.2 it is shown that there is a potential dependence of the adsorption of SPS, the model thickness curve at  $-0.65 V_{MSE}$  reflecting a limiting thickness of  $0.5 \text{ nm} \pm 0.15 \text{ nm}$  versus  $0.8 \text{ nm} \pm 0.15 \text{ nm}$  at the more negative potentials. No potential dependence was found for MPS, with the limiting model thickness of the adsorbed layer 1.1 nm, regardless of potential. Upon examination of the interplay between PEG, Cl<sup>-</sup> and SPS in the bath, it was seen that SPS adsorption was more significant on a shorter time scale at more negative potentials. These findings provide insight as to how potential can play an

important role in formulation of electrochemical baths/processes with greater dynamic range needed to superconformally fill vias and trenches with greater aspect ratios as feature sizes shrink.

**Future Plans:** There are no future plans to continue this work.

**Publications:** The following are publications associated with this work.

1. Walker, M. L., Richter, L. J., and Moffat, T. P., "Competitive Adsorption of PEG,  $\text{Cl}^-$ , and SPS/MPS: an In-situ Ellipsometric Study on Cu", J. Electrochem. Soc. 153, C557-C561 (2006).
2. Walker, M. L., Richter, L. J., and Moffat, T. P., "Potential Dependence of Competitive Adsorption of PEG,  $\text{Cl}^-$ , and SPS/MPS on Cu: An *in-situ* Ellipsometric Study", J. Electrochem. Soc., in press.

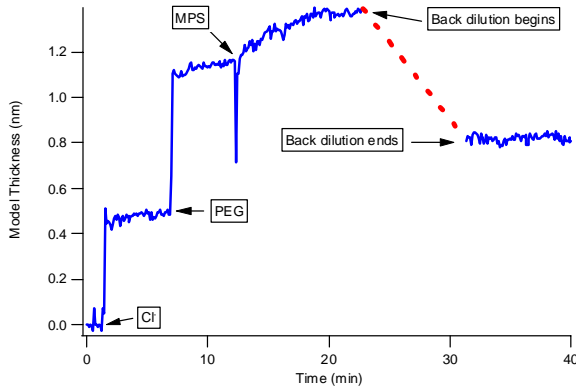


Fig. 1.  $\text{Cl}^-$ /PEG displacement by MPS.  $\text{Cl}^-$  added at 2 min, PEG at 7 min, MPS at 13 min. Back dilution began at 24 min, resulting in a model thickness nearly comparable to MPS limiting value.

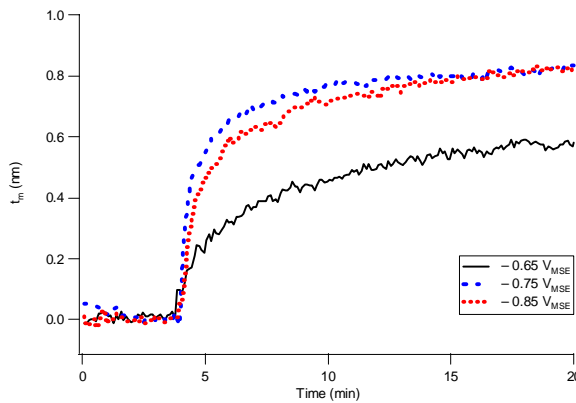


Fig. 2. SPS adsorption as a function of potential.

## Title: Ultra-High Resolution Structured-Illumination Microscopy

Authors: M.R. Beversluis and S.J. Stranick

**Purpose:** Light microscopy is a widely used analytical tool because it provides non-destructive, real-time, three-dimensional imaging with chemically-specific contrast. However diffraction effects typically blur the resolution of these microscopes to 200 nm or worse, which limits their utility for the study of nanoscale materials. Structured-illumination microscopy is a recently developed technique that uses Moiré patterns to provide super-resolving imaging. By taking advantage of the aliasing effect that occurs when a sample is illuminated with a fine sinusoidal pattern, a synthetic image can be formed from a series of Moiré patterns that effectively doubles the resolution of the original image. Our work has taken this technique and applied it using ultra-high 1.65 numerical aperture (NA) objectives to record sub-100 nm resolution images in the far field of single quantum dots and fluorescently-stained biological samples.

**Major Accomplishments:** The finest possible sinusoidal pattern that can be imaged onto a sample using a microscope objective has a pitch  $d$  given by  $\lambda_{ex}/(4\pi \cdot NA)$ , where  $\lambda_{ex}$  is the excitation wavelength. In principal,  $d$  could be made very small using ultraviolet wavelengths, but many fluorescent samples require visible or blue excitation light (nominally 500 nm), which means that increasing the NA is the only practical avenue to higher resolution. Recently, a new objective became available that uses high-optical index glass to achieve a 1.65 NA, which is 17% larger than was previously available.

We developed a structured-illumination microscope based on this objective that achieves a resolution of 75 nm using 488 nm excitation. The resolution was measured using the full-width at half-maximum (FWHM) of single quantum dot images. Figure 1 shows a comparison between the conventional image, which has a FWHM of 195 nm, and the structured illumination technique with a FWHM of 75 nm.

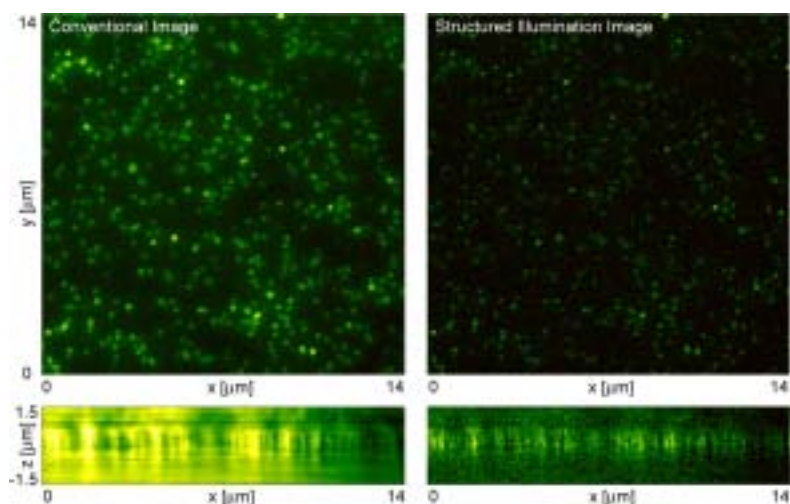


**Fig. 1.** Shown here are convention and superresolving fluorescence images of single green-emitting quantum dots taken using a 1.65 NA structured-illumination microscope.

The bottom two panels in Figure 1 are side views of the image plane. The comparison between the conventional and structured-illumination images shows the improvement for both lateral and axial resolution.

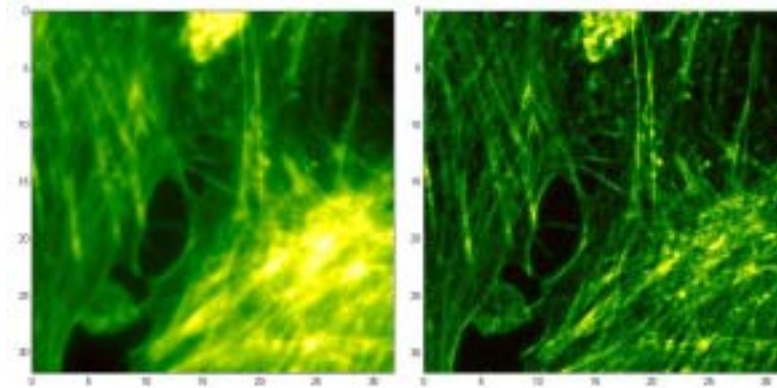


**Fig. 2.** Fluorescently stained bovine endothelial cells imaged conventionally and with the use of structured-illumination. The scale is provided in microns.

Figure 2 shows the results of this technique for a biological sample. In this case, the optical sectioning along the z-axis can be of major help in rejecting out-of-focus light.

**Future Plans:** The fluorescence microscope is now developed to a point where it can be applied to problems in microbiology, and work is currently underway in the study of nanoparticle accumulation in bacteria. Of particular interest is the extension of resolution enhancement to contrast mechanisms based on intrinsic chemical contrast, like the spectroscopic fingerprint that spontaneous and coherent Raman scattering can provide for non-labeled samples. Generally speaking, these techniques require the use of a scanning laser microscope due to their use of high-excitation power levels. To meet this need, we are developing a hybrid technique that uses sinusoidal modulation of a laser beam during the raster-scanning image acquisition. Using this approach, it should be possible to provide sub-100 nm resolution at a cost of a three-time increase in image acquisition time over conventional imaging.

**Publication:** A manuscript entitled “Benchmarking the Performance of Ultra-High Numerical Aperture Objectives for Structured Illumination Fluorescence Microscopy” is currently in preparation.

## **Title: Direct Detection of O<sub>2</sub> in Aqueous Solution for Bioimaging**

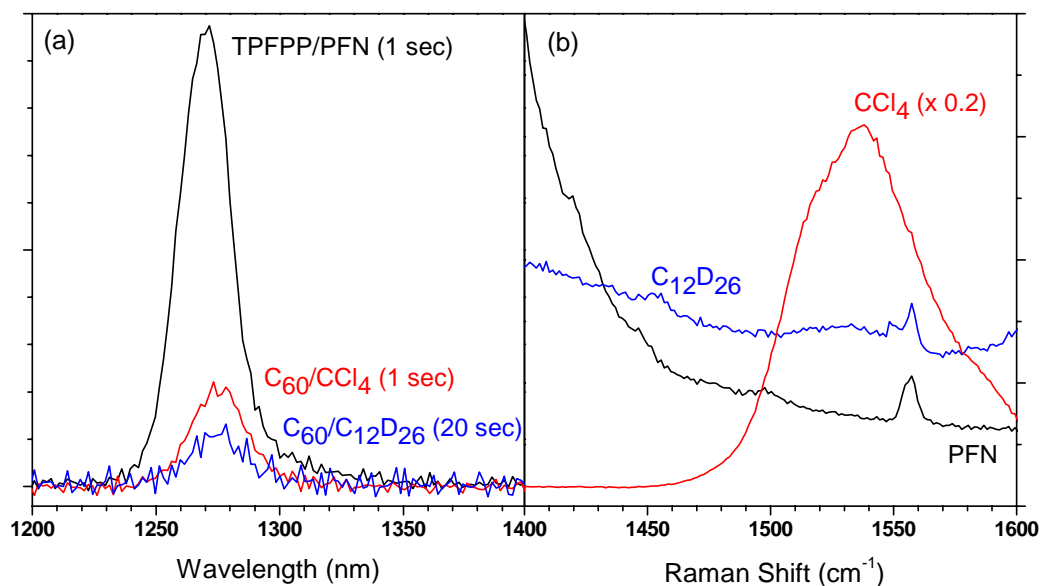
**Authors:** S.A. Buntin, M.R. Beversluis and S.J. Stranick

**Purpose:** Imaging modalities in biological systems generally can be divided into two classifications: “whole body” – where contrast is sought in macro-scale systems (i.e., organs to organisms) and “cellular” – where contrast at micrometer (and less) length scales are used to probe specific regions within cellular structures. While fluorescence based bioimaging has provided a wealth of valuable information with respect to biosystems, there is a great need to develop cellular level *chemical* imaging, where extrinsic contrast agents (i.e., dyes and stains) are not needed and more specific detail can be provided with respect to inherent/intrinsic chemical functional groups. In recent years, coherent anti-Stokes Raman scattering (CARS) has emerged as an innovative chemical imaging technique for biosystems, with sensitivities in some cases (typically “majority” species – e.g., CH<sub>x</sub> in lipids) allowing for video rate (i.e., real time) imaging. The primary goals of this exploratory research project were to 1) develop a CARS spectroscopy/microscopy system, and 2) evaluate the use of CARS in the detection of “minority” species, specifically focusing on O<sub>2</sub>, in biological systems. Ultimately, if favorable characteristic detection sensitivities are apparent, this CARS capability would be directed towards the measurement of singlet O<sub>2</sub> [O<sub>2</sub>(<sup>1</sup>Δ)], which is an unstable, highly reactive species that is critical in photodynamic therapy.

**Major Accomplishments.** Over the last decade, two primary configurations have been developed for CARS bioimaging, with each having attributes that (somewhat) favor different applications. The most “typical” CARS configuration uses two picosecond lasers, and this is well-suited for applications targeting signal maximization from a vibrational resonance at a specific frequency. With this, a single channel detector can be used and video rate, species-specific imaging is feasible. Alternatively, broadband CARS can be performed using a femtosecond and a picosecond laser. This scheme allows for the acquisition of a CARS spectrum for each pulse pair (i.e., “shot”), with the spectral coverage determined by the bandwidth of the femtosecond pulse (can approach 2000 cm<sup>-1</sup>). Further, for both schemes, there are a number of experimental conditions that allow for significant performance enhancements, with one of the most advantageous being the use of well-defined and optimal polarization states for input and output beams, so called P-CARS (Polarization-CARS). In P-CARS, the polarization conditions can be fixed to quite effectively eliminate large detrimental nonresonant signals, which can be orders of magnitude greater than targeted resonant signals for weak/dilute vibrational features. Our work thus far has focused on P-CARS using two picosecond pulses, with spectra over small a frequency interval (several 10’s cm<sup>-1</sup>) obtained via wavelength scanning one of the lasers. We have obtained P-CARS spectra of minor solvent bands, and are currently working towards the detection of dissolved O<sub>2</sub>, which based on spontaneous Raman results has an intensity that is substantially smaller (i.e., > x10) than indicated solvent features.

Concurrent with our development of a P-CARS system, we have determined a sample solution for the production O<sub>2</sub>(<sup>1</sup>Δ) that will serve as testbed for the feasibility of CARS detection of this species. O<sub>2</sub>(<sup>1</sup>Δ) can be effectively formed from ground state O<sub>2</sub>(<sup>3</sup>Σ) via interaction with a photosensitizer (PS), and the O<sub>2</sub>(<sup>1</sup>Δ) concentration is proportional to the <sup>1</sup>Δ → <sup>3</sup>Σ emission intensity at 1270 nm (NIR). A number of PS/solvents systems were evaluated with the primary criteria being 1) insignificant solvent vibrational features determined via spontaneous Raman at

about  $1480\text{ cm}^{-1}$  and  $1555\text{ cm}^{-1}$  to minimize interferences with  $\text{O}_2(^1\Delta)$  and  $\text{O}_2(^3\Sigma)$  and 2) maximize steady state concentration of  $^1\Delta$  determined from NIR emission. It is known that  $\text{O}_2$  has high solubility in nonpolar solvents, and deuterated/fluorinated solvents provide minimal spectral interferences and typically afford long emission lifetimes for  $\text{O}_2(^1\Delta)$ . It was found that tetra(perfluoropropyl) porphyrin (TPFPP)/perfluorononane (PFN) gave the highest NIR emission. In general,  $\text{C}_{60}$ /perdeuteroalkanes provided about  $\times 100$  less  $^1\Delta$  NIR emission than the TPFPP/PFN system and emission for Methylene Blue/ $\text{D}_2\text{O}$  was below the detection limit.



The NIR emission of three PS/solvent systems is shown in (a) with respective integration times indicating the dynamic range of the observed ( $^1\Delta$ ) $\text{O}_2$  concentrations. Raman spectra of the neat solvents in (b) show the extent of interferences; the  $\text{CCl}_4$  spectrum has been multiplied by 0.2 and the peak at  $1555\text{ cm}^{-1}$  in both PFN and  $\text{C}_{12}\text{D}_{26}$  is dissolved oxygen.

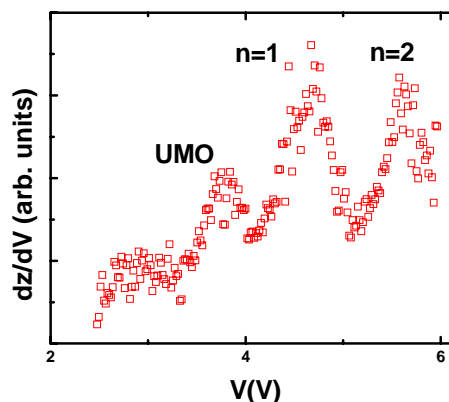
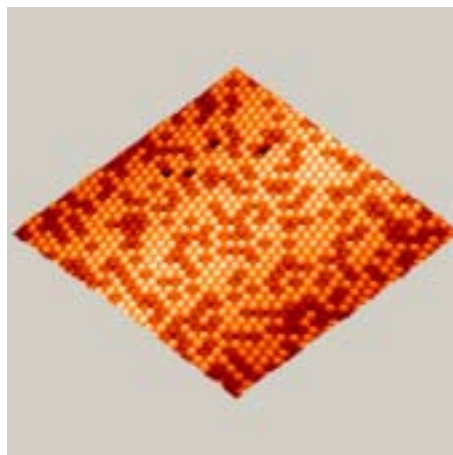
**Future Plans:** We plan to continue to optimize the performance of the CARS configuration towards the development of both video rate imaging of majority species as well as a probe of the spatial distribution of minority species in biosystems. This capability will also be extended to address metrology needs in materials science/reliability, including for example the determination of stress fields with micrometer resolution.

## Title: Nanoscale Electronic Structure Measurements in Organic Systems

**Authors:** D. Dougherty, S.W. Robey, G. Dutton (University of Maryland) and J.E. Reutt-Robey (University of Maryland)

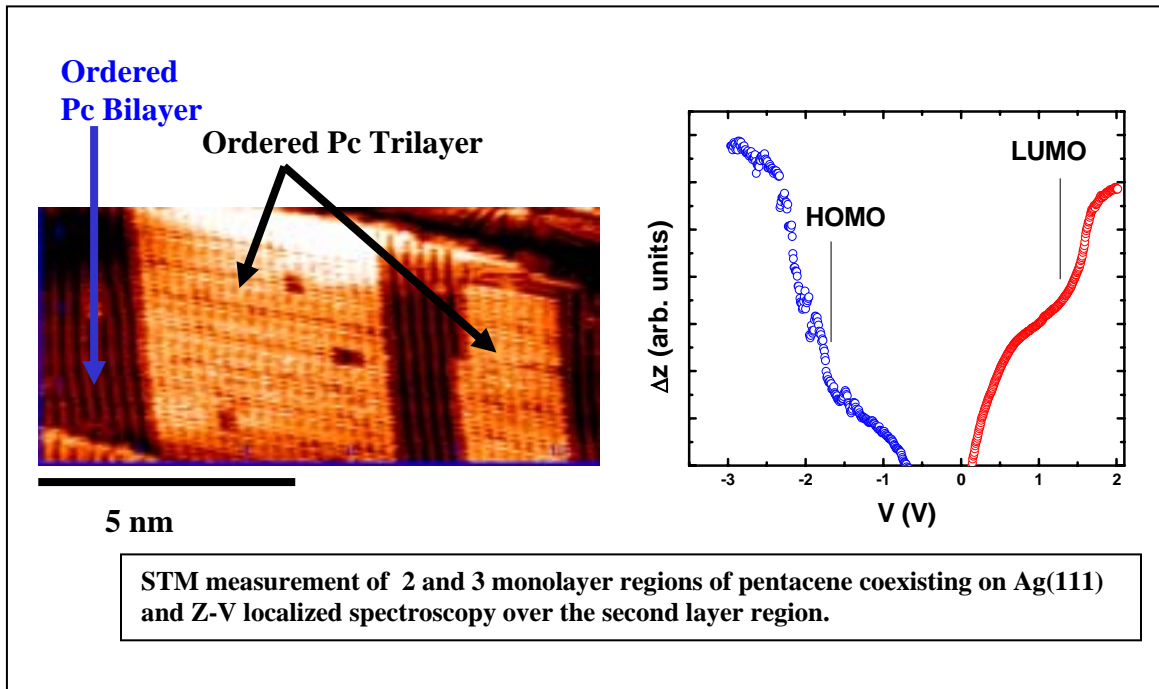
**Purpose:** Knowledge of interfacial electronic structure at organic-metal and organic-organic heterojunctions is a prerequisite for the development of a wide range of organic electronic applications, including organic light emitting diodes, organic photovoltaics, and field effect transistors. Photoelectron spectroscopies can provide this information and have been used extensively for this purpose. However, many advanced applications depend on nanostructured materials and it is desirable to access electronic structure information at nanometer length scales. One technique employed for this purpose is scanning tunneling spectroscopy (STS). Current versus voltage ( $I-V$ ) curves are acquired with sub-nanometer resolution over a fixed location using a scanning tunneling microscope (STM). To perform the measurement the STM tip height is fixed (tip feedback is disengaged) and the voltage between the tip and sample is varied. Current increases occur whenever the voltage corresponds to filled or empty (depending on the bias direction) electronic level. This technique, however, has limitations for molecular/organic systems due to the rapidly increasing current in the system as the voltage is ramped through the experimentally interesting regime. This can lead to breakdown of the molecule/organic or induced molecular motion and make measurements at high bias extremely difficult.

**Major Accomplishments:** In collaboration with researchers at the University of Maryland we are investigating an alternative technique to provide information on localized electronic structure in molecular and organic systems based on tip height ( $Z$ ) versus voltage measurements ( $Z-V$ ).<sup>[1,2]</sup> In this case, the STM tip feedback is engaged at a chosen current setpoint. The voltage in the tunneling gap is then varied as in the  $I-V$  measurement but the feedback now keeps the current constant, causing the tip to retract abruptly at voltages corresponding to molecular resonances. The exponential dependence of the tunneling current on the tip-sample separation leads to small variations in  $Z$  which are monitored. The constant current negates the limitations of  $I-V$  spectroscopy noted above.



STM images of one monolayer of  $C_{60}$  on Ag(111) and corresponding localized unoccupied electronic structure measured using  $Z-V$  spectroscopy. UMO=unoccupied molecular orbital;  $n=1, 2$  are tentatively assigned to image state resonances.

The figures provide sample STM data and preliminary Z-V measurements for thin layers of  $C_{60}$  and pentacene grown on a silver substrate. These molecular materials are of interest for a variety of applications, including photovoltaics and organic field effect transistors.



**Future Work:** Z-V spectroscopy will be used to investigate the localized electronic structure in the vicinity of interfaces between  $C_{60}$  and pentacene and other organic donor-acceptor systems of interest for photovoltaic applications. This information can then be correlated directly to molecular resolved structural information to determine the impact of molecular structure at the interface on donor-acceptor band offsets.

[1] G. Binnig, K.H. Frank, H. Fuchs, N. Garcia, B. Reihl, H. Rohrer, F. Salvan, and A.R. Williams, Phys. Rev. Lett. 55 (1985) 991.

[2] S.F. Alvarado, P.F. Sedler, D.G. Lidzey, and D.D.C. Bradley, Phys. Rev. Lett. 81 (1998) 1082.

## **Title: Vibrational Spectroscopic Characterization of Model Biomembranes**

**Authors:** Z.D. Schultz, S.J. Stranick and I.W. Levin (NIH, National Institute of Diabetes and Digestive and Kidney Diseases)

**Purpose:** The behavior of lipids in biological membranes is important in a variety of biological functions. For example, how lipids organize permits transport across the membrane and the relationship between lipids and proteins is involved in signaling and recognition. Numerous lipids are found in cellular membranes, and the distribution of these lipids in the membrane is somewhat controversial. The existence of heterogeneous lipid microdomains in cell membranes, also called lipid rafts, was initially hypothesized to explain detergent insoluble portions of cell membranes. Skepticism of these rafts is often associated with large disparities in size reported for these raft domains, ranging from a few nm to  $\mu\text{m}$ . One problem in characterizing microdomains is the potential for fluorophores and other exogenous probes to induce aggregation. Infrared spectroscopy offers a label free method to determine the size of these raft domains from splitting in the  $\text{CH}_2$  scissor mode. Lipids, reported to form rafts in biological membranes, are combined into aqueous dispersions, homogenized and allowed to self assemble into lamellar bilayer stacks. The stacks can be conceptualized as a series of bilayers stacked on top of each other with water between. By rapidly cooling the stacks, the lipid distributions that form at elevated temperatures can be trapped in the gel phase. Furthermore, at lower temperatures the lipids can be annealed into an orthorhombic packing configuration where correlation field splitting is evident. These stacks increase the number of molecules being investigated compared to single bilayers, facilitating measurement for weak vibrational signals like the  $\text{CH}_2$  scissor mode. To distinguish between the different lipids in the dispersion, a raft marker is chosen with a saturated, perdeuterated chain. In our experiments we use perdeuterated galactocerebroside as our raft marker. Galactocerebroside is a glycosphingolipid, a class of molecules associated with rafts in vivo. Isotopic substitution permits discrimination of the field correlation splitting associated with the raft marker from other vibrational signals. The field correlation splitting is dependent on the number of chains in the cluster. The formation and size of these domains is then evaluated with respect to changing the components of the model membrane.

**Major Accomplishments:** To date we have successfully measured band splitting associated with the  $\text{CD}_2$  scissor mode of the perdeuterated galactocerebroside (GalCer) in two different lipid matrices: dipalmitoylphosphatidylcholine (DPPC) and DPPC with cholesterol. Shown in Figure 1 are the  $\text{CD}_2$  scissor bands and the second derivatives obtained from GalCer and DPPC (Fig. 1a) and DPPC-Cholesterol (Fig. 1b) matrices. The second derivative is used for determining peak separation of the overlapping bands. For a 1:1 mixture of GalCer and DPPC (Fig. 1a), a splitting  $\Delta\nu = 7.1 \text{ cm}^{-1} \pm 0.1 \text{ cm}^{-1}$  is observed. The addition of 0.6 mol fraction Cholesterol (Fig. 1b) to the sample results in a splitting of  $\Delta\nu = 6.6 \text{ cm}^{-1} \pm 0.1 \text{ cm}^{-1}$ .

$$N = \left[ \frac{\pi}{\sqrt{2(1 - \Delta\nu/\Delta\nu_0)} - 1} \right]^2 \quad \text{Eq. 1}$$

Using Eq 1, and referencing to the splitting ( $\Delta\nu_0 = 7.5 \text{ cm}^{-1} \pm 0.1 \text{ cm}^{-1}$ ) obtained for a pure layer of the perdeuterated chain (d70-distearoylphosphatidylcholine, DSPC), the number of interacting chains is calculated to be 74 in the GalCer-DPPC mixture and decreases to 29 in the presence of 0.6 mol fraction cholesterol. This model assumes two chains per lipid, but since our raft marker has only one perdeuterated chain, the number of lipids in each aggregate is doubled, giving 148 and 58, respectively. Assuming a head group size of 5 nm and a square geometry, this supports aggregates 85 and 50 nm in diameter respectively. This is approximation is in agreement with small rafts predicted from fluorescence measurements. Interestingly, our results support previous reports by others that the addition of cholesterol decreases the size of lipid rafts.

**Future Plans:** This methodology provides the basis for exploring more complex systems associated with cellular membranes. The incorporation of membrane spanning proteins and the inclusion of unsaturated lipids will help elucidate fundamental interactions of biomembranes. Using model systems to understand basic interactions will be helpful in explaining distributions and behavior observed in intact cellular membranes. The project is a first step in using vibrational spectroscopy as a label free method of investigating biological membranes. Future efforts will include more complex systems and imaging experiments on intact membranes.

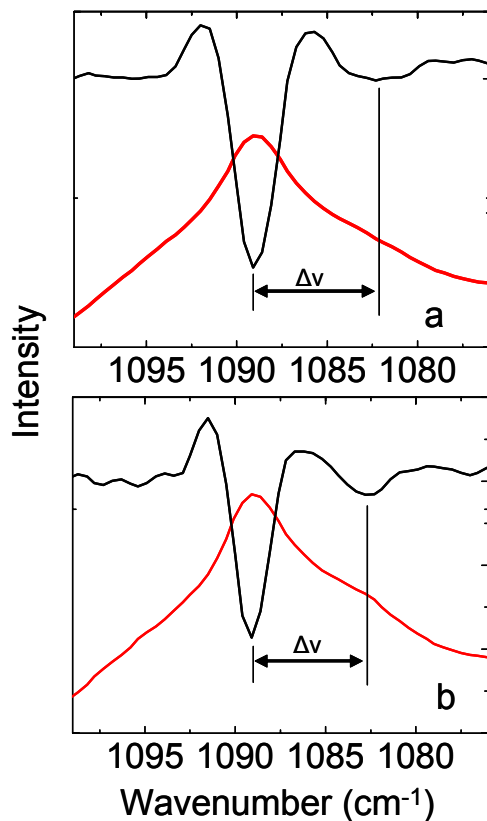


**Figure 1.** Infrared absorption spectra (red) and second derivatives (black) obtained from (a) 1:1 DPPC - Galactocerebroside sample and (b) 1:1:0.6 DPPC-Galactocerebroside-Cholesterol mixtures. Lines are drawn to guide the eyes with respect to the observed splitting.

## FY2007 Technical Activity Report

Dale E. Newbury

Progress in high speed energy dispersive x-ray spectrometry with the silicon drift detector (SDD): 1 MHz output count rate with resolution better than 140 eV!

The silicon drift detector (SDD) continues to make extraordinary advances in energy dispersive x-ray spectrometry (EDS) performance compared to the conventional Si(Li) detector. For all but one major performance criterion (the inevitably decreased efficiency of the 0.3 mm thick SDD for high energy photons above 12 keV compared to the 3 mm thick Si(Li)), the SDD equals or betters the Si(Li), despite operating at -30 °C with Peltier cooling and passive radiative exhaust compared to -190 °C for the Si(Li) with liquid nitrogen cooling. The SDD has superior resolution performance for the same active detector area (e.g., measured at MnK $\alpha$ , 127 eV vs. 129 eV for a 10 mm<sup>2</sup> detector; 134 eV vs. 140 eV for 50 mm<sup>2</sup>). Most importantly, the SDD achieves a given resolution with a much shorter peaking time, which translates into a higher maximum in the curve of output count rate (OCR) vs. input count rate (ICR). In our previous work with the SDD, a maximum OCR of 14 kHz was achieved with the “best resolution” (134 eV) peaking time of 8 microseconds, which can be compared to the Si(Li) OCR of 1.8 kHz with a 50  $\mu$ s peaking time for the same resolution. An unexpected advance in SDD technology has now resulted in a “best resolution” peaking time of 400 ns (for a 10 mm<sup>2</sup> SDD with on-chip first stage amplifier), which gives a maximum OCR above 250 kHz with a resolution of 131 eV. By ganging four of these detectors and multiplexing the signal stream, a combined OCR of 1 MHz can be achieved while retaining resolution below 140 eV for the combined signals of four detectors. This extraordinary OCR performance permits useful x-ray spectrum imaging (e.g., 100 x 100 pixel scan; 1 ms pixel dwell) in only 10 seconds per field of view, while achieving detection sensitivity to all major constituents (concentration greater than 0.1 mass fraction) as well as some minor constituents. Such high speed image data acquisition opens up new applications in microstructural characterization and particle analysis. For example, an x-ray spectrum image can be recorded for each particle, enabling the analyst to make explicit corrections for particle geometry effects that compromise quantification procedures when single point spectra are used. Inhomogeneous particles can be directly recognized in the x-ray spectrum image, information that is inevitably lost when particle overscan spectrum acquisition is used.

## **Title: 3D Molecular Bioimaging Mass Spectrometry**

**Authors:** Greg Gillen, Chris Szakal, Albert Fahey, and Christine Mahoney (837)

**Context:** In recent years, the use of cluster primary ion projectiles for organic secondary ion mass spectrometry (SIMS) has generated considerable interest as a method to improve molecular secondary ion yields, facilitate improved sensitivity for large molecule analysis and minimize the accumulation of beam-induced damage in selected organic materials. In this work, we report on our attempts to combine SF<sub>5</sub><sup>+</sup> primary ion bombardment with secondary ion imaging on an ion microscope SIMS instrument to produce spatially resolved molecular information as a function of depth. Three dimensional (3D) molecular imaging SIMS is achieved by acquiring a series of characteristic *molecular* secondary ion images as a function of increasing depth during dynamic SIMS sputtering of thin molecular films using cluster primary ion bombardment. Reconstruction of the resulting image stack provides a 3D volumetric image of the molecular composition of the sample. This approach has been used to examine several different types of samples including thin polymer films, multilayer polymer films, polymer films doped with pharmaceuticals and biological thin sections.

**Major Accomplishment:** 3D SIMS images have been obtained on the NIST ion microscope SIMS instrument using an SF<sub>5</sub><sup>+</sup> primary ion beam. Microscope imaging is particularly suited for use with cluster ion beam sources because the requirement for a highly focused primary ion beam is eliminated. This allows large diameter, higher current and lower impact energy cluster ion beams to be used which in turn allows for higher sputtering rates, faster analysis times and increased depth resolution. Also, image acquisition rates can be further increased since the secondary ion signal from each pixel in the image is acquired and digitized in parallel. An example of microscope-based molecular image depth profiling is shown in Fig. 1. for a 5 micrometer thick rat brain section on silicon. In this example we show the cluster SIMS mass spectrum for the tissue section which demonstrates a high signal for the m/z 184 phosphatidylcholine molecular ion. Phosphatidylcholine is a phospholipid that is a major constituent of brain tissue. The distribution of this compounds was mapped by acquiring a series of images as a function of increased sputter time into the tissue sample. No degradation in molecular ion signal was observed during the analysis. In this example, the phosphotidylcholine was non uniformly distributed as a function of depth and was anticorrelated with the cholesterol molecular ion distribution (data not shown).

**Future Plans:** SF<sub>5</sub><sup>+</sup> molecular image depth profiling has been demonstrated for a series of polymer films, polymer bilayers, patterned polymer films, polymers containing organic molecules and biological tissues. We plan to extend this work to study imaging of biomarkers within individual cancer cells grown from culture for early cancer detection. This capability will be enhanced by the addition of a C<sub>60</sub> cluster ion source for molecular depth profiling of biological tissue samples.

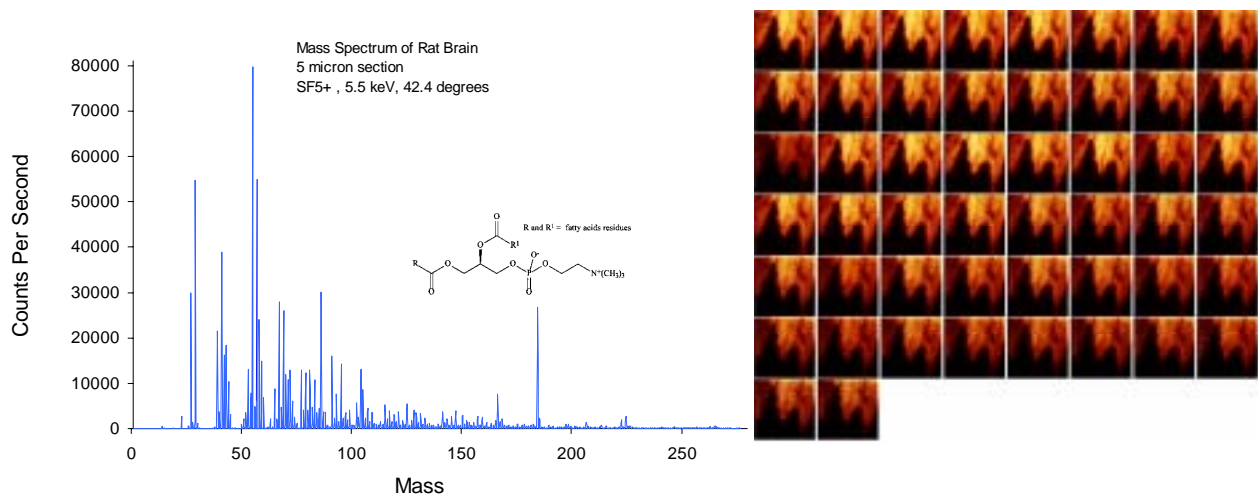


Fig. 1(left). SIMS mass spectrum of rat brain section showing the high yield of the characteristic parent ion at  $m/z$  184 for phosphatidylcholine. Secondary ion image stack of the phosphatidylcholine molecular ion distribution as a function of time through a 5 micrometer thick rat brain section. Each image acquisition was 10 seconds with a 500 micrometer field-of-view. The cholesterol distribution (not shown) was anti correlated with the phosphatidylcholine images.

## Title: Searching for Particulate Nuclear Material Over Large Areas with a High Performance Secondary Ion Mass Spectrometer

**Authors:** Albert J. Fahey, David S. Simons, and John D. Fassett. (837.05)

**Purpose:** The evaluation of samples collected by the International Atomic Energy Agency (IAEA) for the presence of nuclear material and determination of the isotopic composition of this material is a key analytical capability used for monitoring signatories of the Nuclear Non-proliferation Treaty. One method of analysis has been the use of conventional magnetic sector secondary ion mass spectrometers (SIMS) to scan prepared samples searching for isotopes of uranium (or other elements of interest) and measuring their isotopic ratios.

Currently we are developing a method to use a large radius SIMS instrument (ims-1270) to perform a similar function. The ims-1270 has a number of performance benefits compared to conventional SIMS instruments including: higher secondary ion transmission, higher mass resolution and a multi-collector secondary ion detection system. These attributes allow us to use this instrument to scan larger areas for multiple masses at faster speeds with greater sensitivity while adding confidence to the identification of the detected species.

**Major Accomplishments:** The figure below shows data from a sample that was scanned for the presence of  $^{235}\text{U}$ . Sample areas somewhat larger than 5 mm x 5 mm can be scanned in ~ 8 hours. Particles located from the image below can be re-located and analyzed further. Up to 5 masses can be monitored simultaneously with no loss in analysis speed compared to more conventional single mass detection systems.

**Future Plans:** Further programming and refinement of this method will be performed in the coming year. Plans exist to expand and enhance the abilities of this new method to provide more information over a larger area of the sample. In addition, we will be testing mixtures of standard particles to gauge the efficacy of the method. Successful implementation of this method will result in significant improvements in analysis speed and sensitivity over current analytical methods used for international treaty verification by the IAEA.

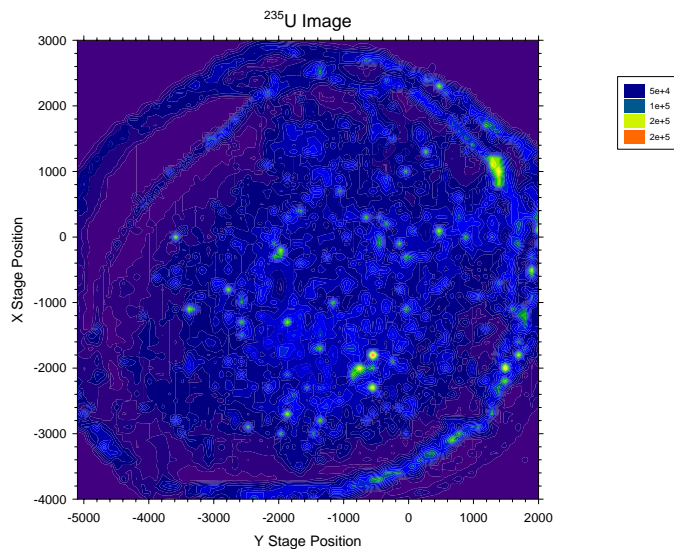


Figure 1. Mass Spectral image of  $^{235}\text{U}$  from large sample area.

# Title: The Use of Inkjet Printing Technology to Produce Standards for Trace Level Explosive Analysis

**Authors:** Eric Windsor, Greg Gillen, and Marcela Najarro (837.05)

**Purpose:** The purpose of this project is to develop a procedure to produce standards for trace explosive analysis. Homeland security priorities have led to the unprecedented deployment of trace level explosive detection systems for counter terrorism purposes. It is estimated that tens of thousands of ion mobility spectrometry (IMS) based instruments are now deployed at airports, seaports, embassies, national monuments and at government and military facilities worldwide.

Standards are needed to calibrate IMS instruments and optimize their performance. Since standards are consumed during IMS analysis, any standards production method must be capable of producing large quantities of standards quickly and inexpensively. To achieve this we are investigating piezoelectric drop-on-demand inkjet printing technology. Piezoelectric inkjet printing is a rapidly expanding technology with diverse applications ranging from the printing of microelectronics to the printing of DNA arrays and tissue engineering. Inkjet printing potentially offers a flexible, rapid and reproducible method for the preparation of explosive standards. These standards can be printed onto a variety of substrates ranging from paper to floppy disks to luggage handles. For standards production, a large dynamic range ( $10^5$ ) in explosive concentration on the printed standards can be achieved from a single standard solution simply by changing the number of droplets printed.

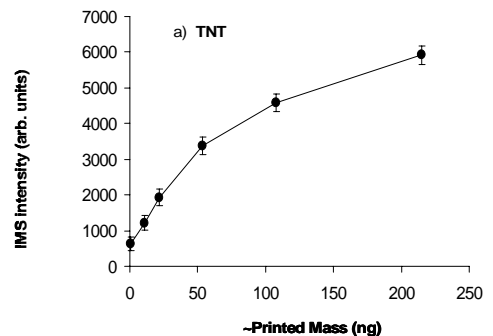
**Major Accomplishments:** The piezoelectric inkjet printer has been used to print a variety of explosives including TNT, RDX and PETN. We have also printed the plastic explosives C4, Semtex and detasheet. A pilot study is underway to evaluate the performance of currently deployed IMS instruments and gain insight into lifetime issues that exist with explosive standards. In this pilot study, prototype standards of C4 explosive were produced using inkjet printing and issued to the U.S. State Department for distribution and testing at U.S. embassies. Additional explosive standards were produced for evaluation by the Transportation Security Laboratory, the National Institutes of Health and NIST.



C4 Prototype standard sheet containing 10 consumable standards.



Fluorescence microscope image of inkjet printed array



IMS response curve for inkjet printed prototype TNT standard

**Future Work:** Future work will include the investigation of methods to improve the lifetime of these semivolatile explosive standards. Methods under consideration include experimentation with different packaging techniques, and methods to encapsulate the explosive including the incorporation of a polymer into the printing solution or the use of surface alteration techniques to encapsulate the explosive.

## Title: Depth profiling of Drug Eluting Stent Coatings with Cluster SIMS

Authors: Christine Mahoney<sup>1</sup>, Albert Fahey<sup>1</sup>, Anna Belu<sup>2\*</sup>

1) Division 837.05, NIST, 2) Medtronic Inc., 710 Medtronic Parkway, LT130, Minneapolis, MN 55432-5604 USA

**Purpose:** There is much excitement in the cardiology community about drug eluting stents (DES), a promising new treatment for coronary artery disease. A coronary stent is a small coiled wire-mesh tube that is inserted into a blood vessel and expanded using a small balloon during an angioplasty procedure. When the balloon is inflated, the stent expands, locks in place and forms a scaffold to hold the artery open, improving blood flow to the heart muscle and decreasing the probability of restenosis or renarrowing of the artery. These stents often incorporate a drug delivery system consisting of a polymeric layer or coating containing a drug, where the drug acts to further prevent the build up of smooth muscle cells on the stent. It is particularly important in DES to characterize the molecular composition of the surface and near surface region of the device (1-500 nm) because this region controls the biocompatibility and influences the magnitude and temporal variation of drug release. Secondary Ion Mass Spectrometry (SIMS) has already proven to be a useful tool in the surface analysis of various drug delivery systems. With SIMS, the molecular distribution of both drugs and excipients within a drug delivery systems can be determined with a high degree of spatial resolution (<1 $\mu$ m) and sensitivity (as low as ppm ( $\mu$ g/g)) when compared to other analytical methods such as Raman and IR spectroscopies. Furthermore, with the advent of polyatomic primary ion sources ( $C_{60}^+$ ,  $Bi_3^+$  and  $SF_5^+$ ), which yield significant improvements in molecular signals (up to 1000 fold increase), and result in decreased beam-induced damage accumulation, it is now possible to obtain 3-dimensional compositional information from model systems, particularly at low temperatures which yield optimum results.

**Major Accomplishments:** Secondary Ion Mass Spectrometry (SIMS) employing an  $SF_5^+$  polyatomic primary ion source for sputtering and  $Bi_3^+$  primary ions for analysis was used to depth profile through DES coatings obtained from Medtronic (DES manufacturer) at variable temperatures. Figure 1 shows the resulting depth profiles of PLGA/Rapamycin films which were prepared by casting solutions of 2% w/v poly(lactic-co-glycolic acid) (PLGA) containing 5% w/w rapamycin (~6  $\mu$ m) onto steel substrates. Figure 1a, shows the resulting depth profile acquired at room temperature. As can be seen, the signal starts to decay at  $SF_5^+$  primary ion doses of  $\sim 1.3 \times 10^{15}$   $SF_5^+$  ions/cm<sup>2</sup> and the steel substrate is never reached. However, as indicated in Figure 1b, the depth profile stability is dramatically improved at low temperatures (-100 °C), as indicated by the relatively constant signal up through  $SF_5^+$  primary ion doses of  $\sim 1.5 \times 10^{16}$   $SF_5^+$  ions/cm<sup>2</sup>. At this dose the secondary ions characteristic of the DES coating start to decrease while the corresponding steel substrate intensities increase, indicating that the entire film has been eroded. This result shows that using low temperatures can extend the utility of  $SF_5^+$  to characterize thicker polymeric materials (6.0  $\mu$ m as opposed to 0.2  $\mu$ m).

Cluster SIMS at low temperatures has also be used to elucidate the 3-dimensional structure in these DES coatings, as illustrated in Figure 2, which shows secondary ion image overlays of  $m/z = 99$  (fragment characteristic of PLGA) and  $m/z = 84$  (fragment characteristic of Rapamycin) in a PLGA film containing 25% rapamycin. These images were acquired as a function of increasing sputter time or depth, and thus give detailed information on the heterogeneity in the surface and near surface region in these systems as

compared to the bulk. To our knowledge, these images represent the first demonstration of successful 3-D SIMS imaging in real world drug delivery devices.

**Future Plans:** We intend to continue our collaborative work with Medtronic and study the 3-D structure in their Drug Eluting Stents as a function of dissolution time in a phosphate buffered saline.

**Related Publications:**

Mahoney, C.M.; Patwardhan, D.V.; McDermott, M.K. *Applied Surface Science*. 2006, 19, 6554-6557.

**Graphs:**

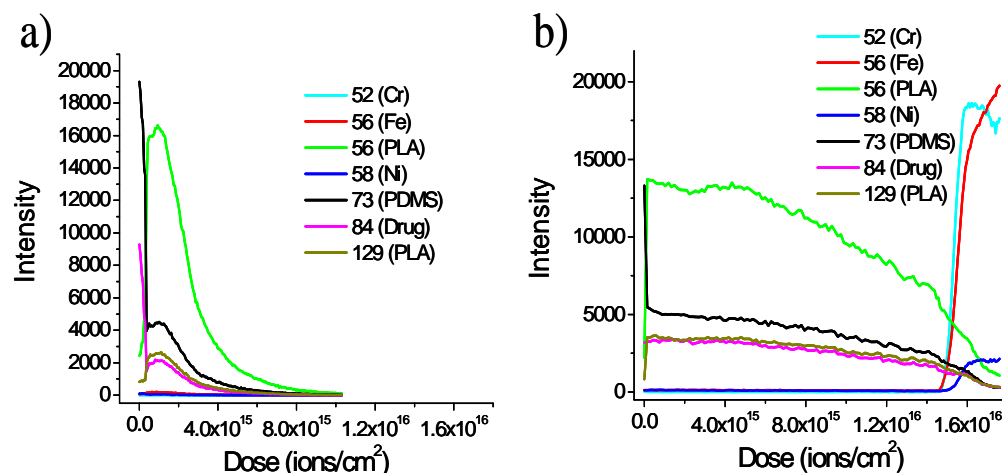


**Figure 1.** Secondary ion intensities plotted as a function of increasing  $SF_5^+$  dose (directly related to depth into film) for a sample of PLGA containing 5 % (w/w) Rapamycin ( $\sim 6 \mu m$ ) coated on steel. Profiles were acquired at: a) 25 °C, and b) -100 °C

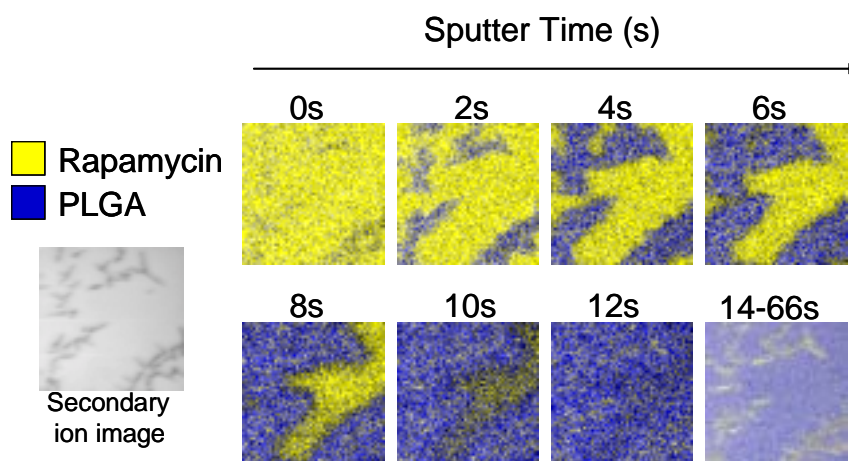


**Figure 2.** Overlay of Secondary ion images acquired as a function of increasing  $SF_5^+$  sputter time (depth) in a PLGA film containing 25% w/w Rapamycin. Blue represents  $m/z = 99$  (PLGA) and yellow represents  $m/z = 84$  (Rapamycin). These images were acquired with a  $Bi_3^+$  cluster primary ion source.

## Title: Robust Spectral Quantification of Large Particle Data Sets

Authors: Nicholas W. M. Ritchie

*Purpose:* Until recently particle analysis with electron beam instruments, while capable of performing small-scale analyses, has been too time consuming to produce statistically significant population data. With the introduction of automated scanning electron microscopes optimized for rapid particle analysis it is now easy to collect ten-thousand particle or larger datasets. The first step in any quantification of a microanalytical spectrum is fitting the spectral peaks with measured or computed elemental reference spectra. Particle spectra are no different in this regard. However, from a practical perspective, the problem differs in both scale and character. When quantifying a small number of spectra it is practical to manually identify a minimal set of elements to fit. When you have hundreds or thousands of particles, this kind of manual effort is not practical. As a result, the analyst must select an exhaustive list of elements to fit against all spectra. The algorithm must then be smart enough to eliminate those elements that are not present based on the statistical evidence. In addition, particle spectra are different from classic bulk spectra. The count statistics in a particle spectrum fall between those of an x-ray map (very poor) and those of a classic microanalytical measurement (high quality.) Because each element can contribute more than one family of x-ray lines, the algorithm must be intelligent enough to consider all lines when making the determination. Yet because particle spectra can look very different from bulk spectra, many rules-of-thumb developed on bulk-spectra sometimes fail. With care, we can identify the presence or absence of elements in the few weight percent levels in spectra with twenty or thirty thousand counts. Finally, the algorithm must be robust enough to produce trustworthy results for thousands of spectra.

Samples run here at NIST and at other labs have identified a weakness in the current method of quantifying particle spectra. NIST as part of our OA program is the primary laboratory leading this new particle analysis methodology, it is our role to develop the algorithms and tools necessary to produce the optimal results.

*Major Accomplishments:* A tool (Graf) has been developed which can reliably process data sets in excess of ten thousand particles against twenty or more elemental references (see Figure 1.) In addition, Graf applies a tool (the max-pixel derived spectrum) developed for x-ray spectral imaging to the particle data set problem to facilitate the identification of the complete element set. This tool has been provided to the OA laboratories.

*Future Plans:* Many of the refinements developed in this project will be able to be applied back to classical electron probe analysis to address the long standing unresolved problem of performing reliable peak identification (qualitative analysis).

*Pubs/Outputs:* The tool (Graf) has been provided to the OA laboratories.

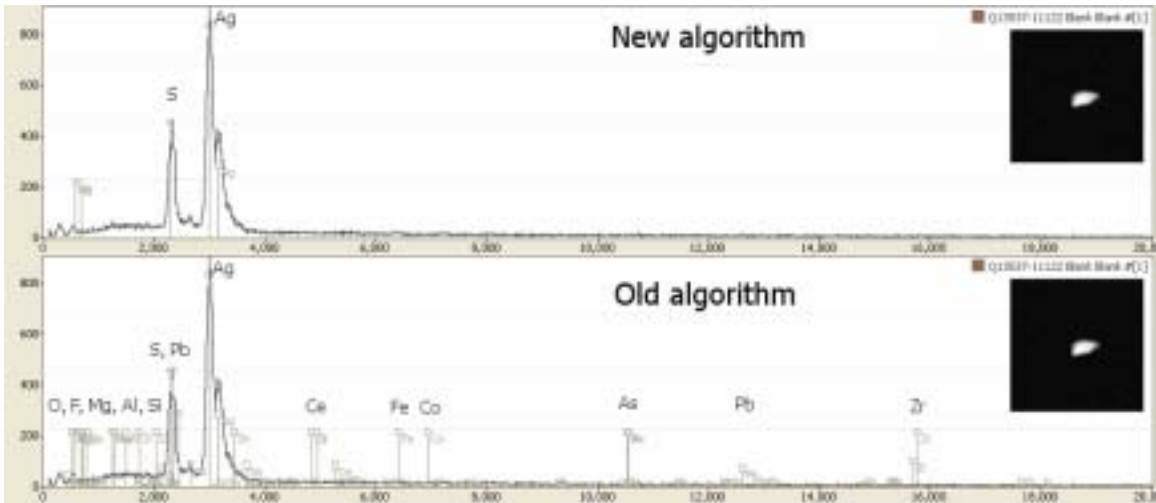


**Figure 1:** Graf spectrum plots showing the new algorithm's improvement over the old algorithm in its ability to discriminate the presence of minor elements. The new algorithm makes full use of the spectrum statistics to eliminate elements which lack sufficient evidence. The new algorithm was able to handle the difficult Pb-S overlap in this silver sulfide ( $\text{Ag}_2\text{S}$ ) particle correctly.

## **Title: Smart Standards: Demonstration of Thermochromic Inks in Trace Explosive Metrology**

**Authors:** R.M. Verkouteren, G. Gillen, R. Rouse (U. Cal. – San Diego, La Jolla, CA), T. Wegener (Gesellschaft für Silizium-Mikrosysteme, Großberkmannsdorf, Germany)

**Purpose:** A “smart” standard will respond interactively with changes in its environment in a functional and predictable manner. These changes may include (but are not limited to) temperature, strain, light, and atmospheric pressure. Smart standards can offer levels of performance beyond those of ordinary standards, in that they offer important operational feedback to a user or instrument that can validate and/or adjust reference values of the process.

Thermochromic inks, which respond either reversibly or non-reversibly to temperature changes, have many practical applications. Reversible thermochromics are widely used as safety devices. They are used on engine parts, fire-resistant doors, and saucepan handles to prevent burns by warning of dangerously high temperatures. Non-reversible thermochromic inks have been used to indicate the maximum temperature which has been experienced by (for example) aluminum gas cylinders or in food packaging. The objective is to produce an historical marking system which will change color irreversibly if the object is at any time stored at too high a temperature. A wide range of thermochromic inks with different temperature transitions has been developed, many in the form of polymers whose response can be adjusted by chemical modification.

This year we have demonstrated the use of thermochromic inks as interactive metrological tools, which can provide “smart” functionality to standard materials now being developed to test the reliability of thousands of trace explosive detectors deployed at airports by the Transportation Security Administration. These detectors utilize thermal desorbers to volatilize residues sampled on a swipe, and the temperature experienced by the residue during desorption is critical to the sensitivity of the trace detection process. Lower temperatures may fail to vaporize the explosive, whereas higher temperatures may cause decomposition. Either result may lead to negative detection of the targeted explosive.

**Major Accomplishments:** The challenge was to spatially distribute a thermochromic ink across a swipe in a precisely positioned array of visible lines or dots, and yet in minute quantities that would not interfere with the normal operation of a trace explosive detector. Several irreversible inks with color transitions (black-to-red and green-to-red) temperatures between 160 °C and 200 °C were procured from Chemsong, Inc. (Chicago, IL). We initially worked with researchers at the University of San Diego (La Jolla) and Großberkmannsdorf, Germany, who have experience in producing intricate arrays on piezoelectric nanoplotter. We were successful in producing arrays of thermochromic inks on several types of swipe media used by manufacturers of trace explosive detectors. Optical microscopy was performed to visualize these thermochromic ink applications, and an example is illustrated in Figure 1.

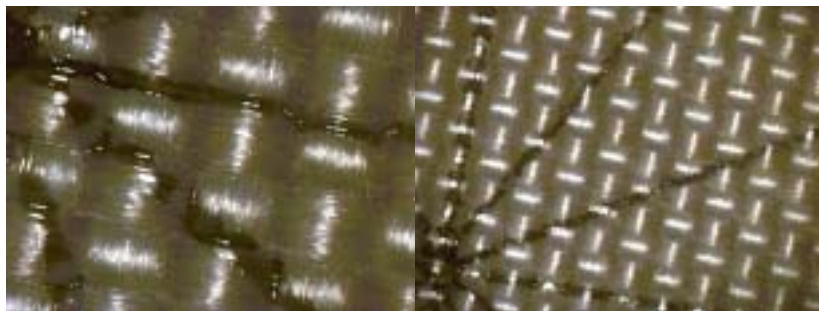


**Fig. 1:** Thermochromic ink plotted as lines (ca. 0.3 mm width) on woven PTFE media used by GE Security.

At NIST, we have compared calligraphy pens, rubber stamps, and inkjet printers to manufacture test swipes that have thermochromic functionality. These were tested on several IMS-based explosive analyzers to establish ink quantities that would not interfere with explosive detection. This quantity corresponded to about 1.0  $\mu\text{L}$  of undiluted ink, applied across the pattern and well dried. For an array of 100 spots, this is 10 nL per spot. We found that only inkjet printers could reliably deposit these small quantities, which amount to a limit of 200 droplets of diluted (1:1) ink per spot using 58  $\mu\text{m}$  diameter droplets.

While manufacturers of detectors indicate the general location of the optimal area (the “sweet spot”) on supplied swipes, the actual location, area, and shape of the true “sweet spot” in a particular detector may be somewhat variable. We designed a pentagonal star-shaped pattern (Fig. 2) that has an inner perimeter surrounding the deposit of trace standard material (not visible). Dotted lines radiate to an outer perimeter, which is about 2.5 cm in diameter and outside the heated area. Upon inspection, the user can verify that the inner perimeter (and sample) was heated to the proper temperature, and trace around the color change limit on each radial line to determine the symmetry of the isotherm.

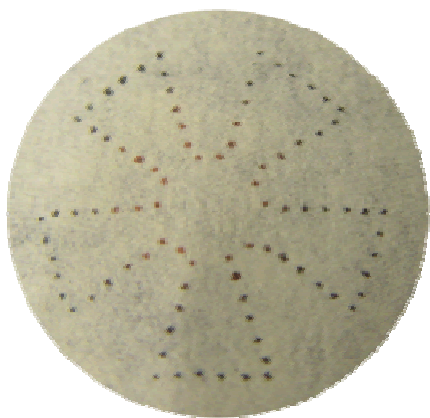


**Fig. 2:** On a swipe, a pentagonal star-shaped pattern of thermochromic microdots is used to test the thermal desorption performance of a trace explosive detector. Here, microdots that reached 200  $^{\circ}\text{C}$  during desorption changed color from black to red, confirming adequate performance.

**Future Plans:** We anticipate that thermochromic inks will be useful in “smart standard” designs, and add value to many testing & evaluation materials. These inks may be printed on media surrounding deposits of standard materials, in order to verify that the target area achieves a specified temperature during thermal desorption. This will also provide a visible indicator for one-use-only media, and indicate whether the media had been improperly stored in a hot environment prior to use. We will investigate formulating thermochromic inks with non-toxic and biodegradable solvents such as ethyl lactate to provide an environmentally benign inkjet fluid.

**Report of Analysis** (*Demonstration of Irreversible Thermochromic Inks in Trace Explosive Metrology*, 837-57-06) to the Transportation Security Administration, NIST Office of Law Enforcement Standards, and the Department of Homeland Security.

**Title:** Aberration-corrected, monochromated analytical electron microscopy

**Author:** John Henry J. Scott

**Purpose:** Since the early days of transmission electron microscopy (TEM) in the 1940s, the resolution of the technique has not been limited by diffraction physics or the wavelength of the electrons, but by the large residual lens defects in the optics, especially spherical and chromatic aberration. Light microscopists solved this problem in the 1820s, and it led immediately to a series of breakthroughs in microbiology and medicine. Duplicating this success has proven extremely difficult for electron microscopy because of the nature of the lenses, and this critical problem remained unsolved for more than 60 years. Recently, solutions for both of these problems have been found and commercialized in a very short span of time, and the field of analytical electron microscopy (AEM) is undergoing the most exciting revolution since its birth. The spatial resolution achievable has already improved to the order of 100 picometers, and will hopefully continue to fall towards the diffraction limit of around 2 pm in the decades to come. CSTL seeks to play a central role in this progress as part of its mission to develop new analytical and imaging techniques and extend the nation's measurement infrastructure in the area of chemical analysis at very high spatial resolution. As expected, application of this technology (even at current levels of performance) has an unusually broad impact on industry, government science and technology functions, and academic research. The areas of advanced materials science and engineering, semiconductor manufacturing, nanotechnology, structural biology, and nanomedicine will benefit immediately from this work.

**Major Accomplishments:** NIST installed the world's first commercial aberration-corrected, monochromated AEM. The information transfer limit for this instrument is below 1 nm in both scanning mode and TEM mode (Figure 1), and establishes NIST as one of the foremost laboratories in the world at atomic resolution chemical analysis.

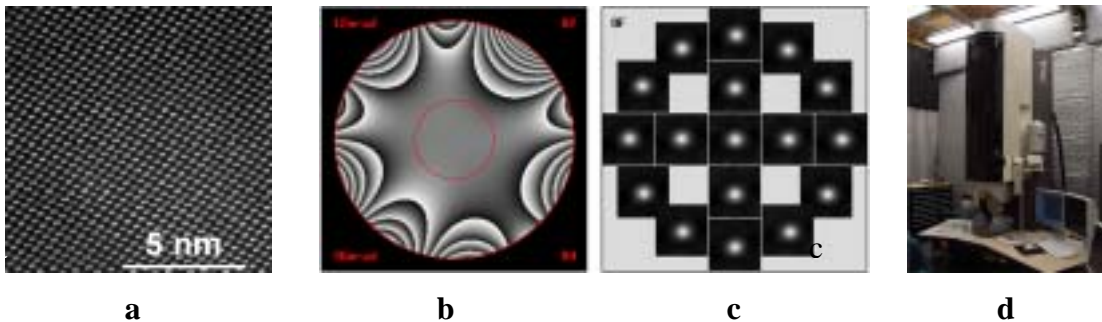


Figure 1: a) Atomic resolution STEM image of silicon b) calculated phase map showing residual lens aberrations, c) Zemlin tilt tableau of the STEM beam used to measure aberrations, d) photograph of the microscope in the Advanced Measurement Laboratory (AML).

**Future Plans:** In addition to further work with the manufacturer and the broader microanalysis community to develop the full potential of this new technology, the microscope will be applied to practical problems such as gate dielectric thickness metrology, and the characterization of dendrimers and heterogeneous nanoparticles for drug delivery.

**Title:** Measuring Pixel Classification Accuracy Using Synthetic Spectrum Images

**Authors:** John Henry J. Scott, Nicholas Ritchie

**Purpose:** The proliferation of commercial microanalysis equipment capable of acquiring electron-excited X-ray spectrum image data in the scanning electron microscope (SEM) has been a boon to researchers and industrial users who rely on X-ray microanalysis to characterize the spatial distribution of elements in solid microstructures. Frequently such systems come with software to classify the pixels in the acquired data cubes into distinct classes or categories. This is a difficult problem because of the physics of the interaction of the electron beam with the sample, differential absorption of the emitted X-rays, and susceptibility of the algorithms to noise. Metrics for measuring the fidelity of these classifiers are non-existent in the microanalysis community, mainly due to the lack of certified reference samples with known spatial phase distributions. Using techniques from the medical imaging community, classification accuracy metrics can be based on synthetic “phantoms”, or artificial datasets with known properties. The availability of such phantoms enables the robust evaluation of classification schemes.

**Major Accomplishments:** Using NISTMonte, an electron-transport and X-ray generation Monte Carlo simulation for complex 3D geometries, full electron-excited X-ray spectrum images were generated for multiphase phantoms (Figure 1). The resulting data cubes are perfectly suited for measuring the accuracy of various pixel classification algorithms currently applied to microanalysis problems.

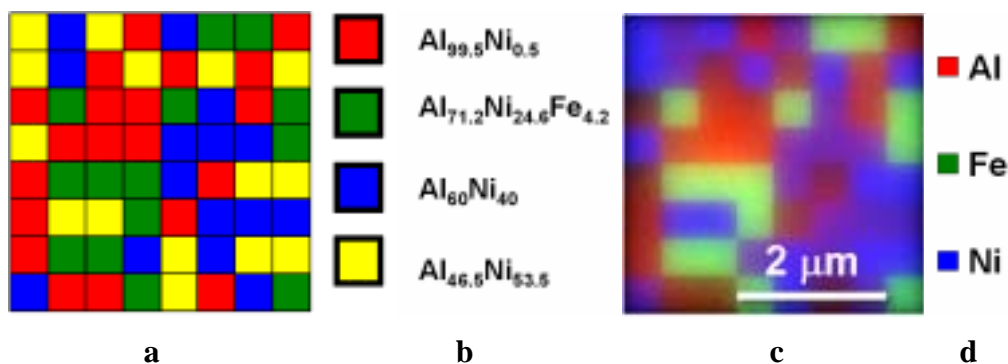


**Figure 1:** a) *in silico* phantom used to generate synthetic spectrum image data, b) legend showing color codes for chemical phases in phantom in (a), c) RGB false color X-ray intensity map derived from simulated spectrum image, d) legend for map in (c), (red, green, blue)=(Al, Fe, Ni) X-rays respectively.

**Future Plans:** Additional spectrum image data cubes will be generated to develop a suite of benchmark problems with known solutions for classification methods. Current and future developers of classifiers can test their code’s performance against their peers and against absolute metrics of interest to end users of the classifiers such as microanalysts.

**Outputs:** JH Scott, N Ritchie, “Measuring Pixel Classification Accuracy Using Synthetic Spectrum Images”, *Microsc. Microanal.* (2006), **12**: 1394-1395.  
doi:10.1017/S1431927606069480.

## **Large Angular Convergence Scanned Beam Illumination (LACSB): Incoherent Imaging for Conventional TEM**

Ian M. Anderson

**Purpose:** The transmission electron microscope (TEM) provides a flexible tool for metrology at spatial resolutions of a nanometer and smaller. In the conventional (CTEM) mode of instrument operation, the specimen is uniformly illuminated with a spread electron beam, and an image is formed with the microscope's objective lens, analogous to optical microscopy. In the scanning (STEM) mode, the electron beam is focused into a small probe, and an image of the specimen is formed by translating the probe across the specimen in a two-dimensional (2D) raster, and displaying the signal of a detector in a synchronous raster. Generally speaking, CTEM techniques are most efficient for [2D] imaging applications, because the many pixels comprising the image are acquired in parallel, whereas STEM techniques are best suited to [1D] profiling and [0D] point analysis, since the pixels must be acquired serially, but the outputs of multiple parallel detectors can be acquired simultaneously. For example, a 256×256-pixel hyperspectral chemical image using electron energy-loss spectroscopy (EELS) can be acquired in minutes by energy-filtered CTEM (EFTEM) using an energy range (0 to 1000 eV) that distinguishes among all elements of the periodic table; the same data acquired using the comparable STEM approach would take hours to achieve comparable statistics. Unfortunately, quantitative CTEM imaging of crystalline specimens is inhibited by diffraction effects – coherent scattering contrast that arises from the dynamical diffraction of the incident probe with atoms arranged on a crystal lattice. Since the vast majority of materials are multiphase and polycrystalline, CTEM-based techniques are unreliable for quantitative imaging studies that capture the relevant microstructure.

**Major Accomplishments:** A method has been developed that damps coherent contrast mechanisms in CTEM imaging, thus removing the “show stopping” obstacle to efficient quantitative chemical imaging at nanometer resolution. The method involves a hybrid mode of instrument operation, in which CTEM imaging is performed while operating the microscope in STEM mode. Coherent contrast is damped by image acquisition over a range of incident beam orientations, thus “averaging out” the unwanted diffraction contrast, so that the bright-field (BF) image exhibits only weak amplitude contrast (Fig 1). The damping of diffraction contrast is dramatically demonstrated in EFTEM  $t/\lambda_p$  mapping, where coherent contrast mechanisms provide a significant artifact, masking the smooth variation in the thickness profile of the wedge-shaped TEM specimen (Fig. 2). This incoherent CTEM imaging method will allow quantitative structural and chemical imaging of nanoscale structures, such as those needed to sustain further improvements in performance in microelectronic devices in the post-CMOS era.

**Future Plans:** The angular variation of the incident beam orientation in a series of fixed-beam TEM images will be explored as the basis for a hyperspectral imaging technique to perform exit-wave reconstruction (EWR), similar to through-focal series reconstruction. Such an approach can be used to damp delocalized coherent contrast and to extend the resolution of TEM imaging from the so-called point resolution (best resolution from a

single, fixed-beam image) to the information limit of the instrument (limited only by incoherent aberrations). Should this approach prove successful, we should be able to demonstrate, for the first time, sub-0.1-nm imaging in both TEM and STEM modes of operation on the same instrument.

**Publications:**

IM Anderson, "A Method for Partially Incoherent Imaging of Crystalline Specimens in Conventional TEM," submitted to Ultramicroscopy, 2006.

IM Anderson, "LACSBI: Incoherent Imaging for Quantitative TEM," in preparation for Microscopy and Microanalysis 13 (Suppl. 2), 2007.

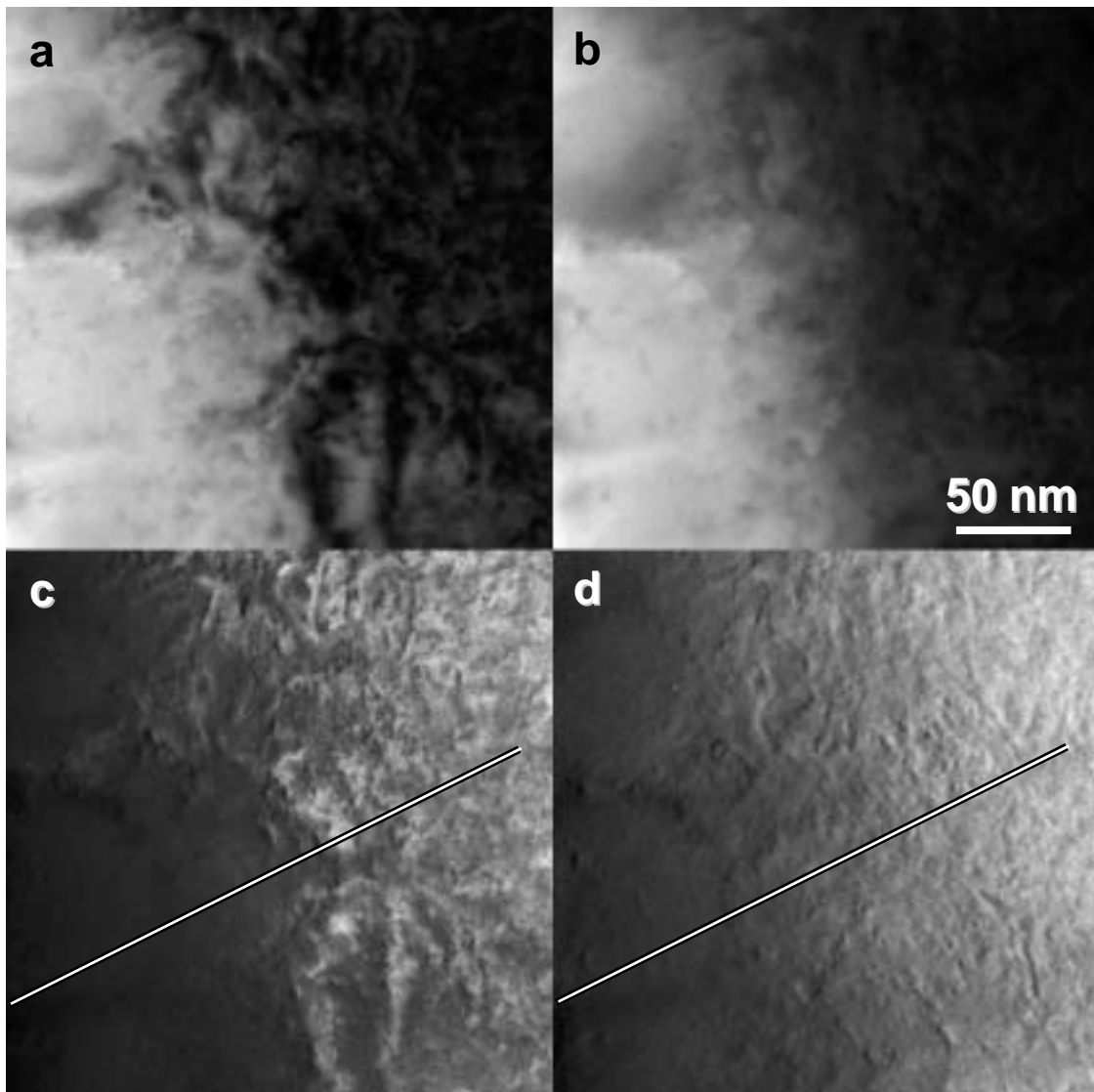


Fig. 1. Mitigation of diffraction effects in LACSBI mode: (a,b) zero-loss bright-field and (c,d) EFTEM  $t / \lambda_p$  images acquired in (a,c) TEM fixed beam and (b,d) LACSBI modes. Profiles corresponding to line shown in (c,d) are shown in Fig. 2.

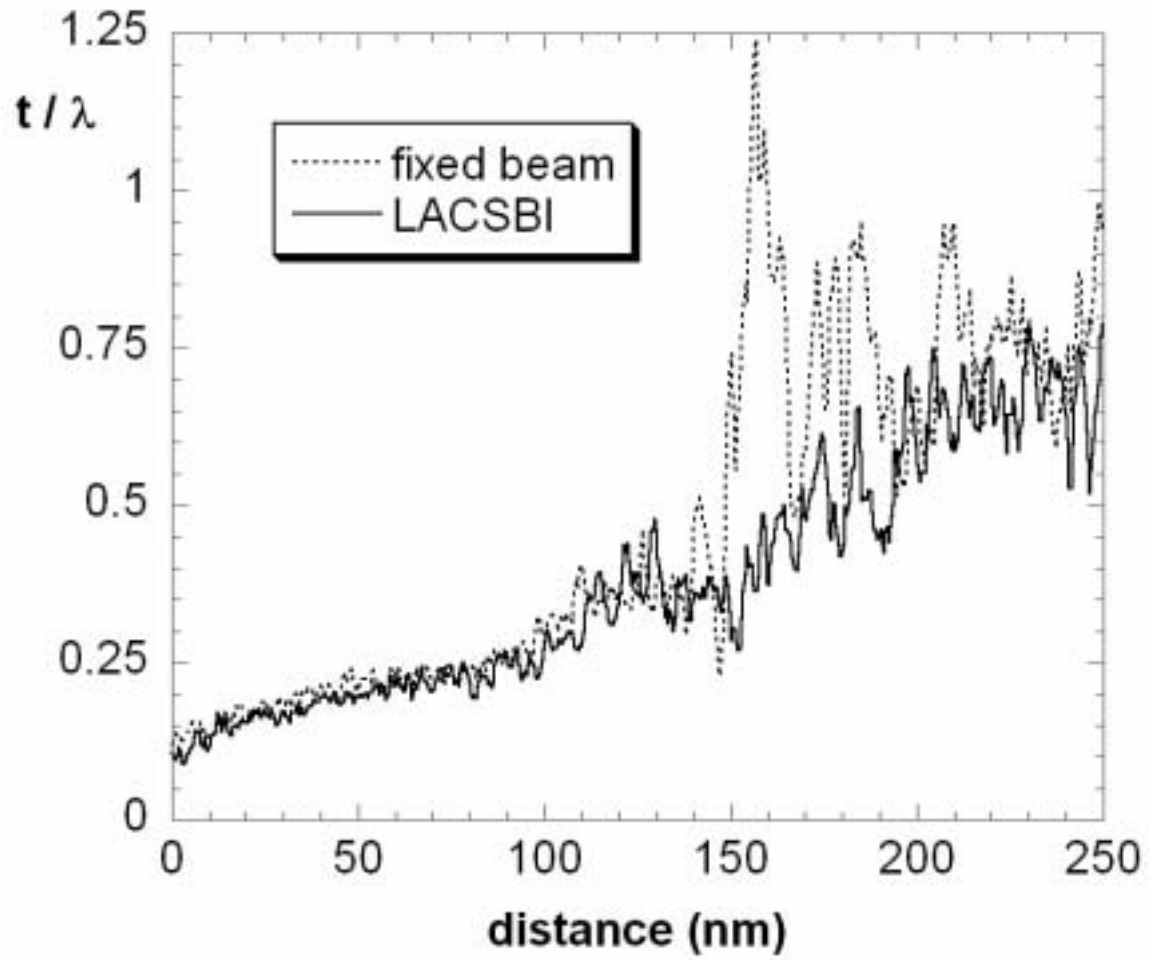


Fig. 2. Plot of  $t/\lambda_p$  as a function of position along the line shown in Figs. 1c,d.

## **Title: Measurement of Uranium Isotopic Composition with High Sensitivity and Specificity by Secondary Ion Mass Spectrometry**

**Authors:** D. S. Simons, A. J. Fahey and J. D. Fassett (837.05)

**Purpose:** Uranium that is highly enriched in the isotope  $^{235}\text{U}$  is a key component of one type of fission-based atomic weapon. Therefore, the measurement of the isotopic composition of uranium is of keen interest to nuclear forensics investigators from organizations such as the International Atomic Energy Agency (IAEA). The IAEA carries out environmental sampling at facilities in its member states with the goal of detecting undeclared uranium enrichment activity. The collected samples are subjected to various screening measurements, the most important of which is the determination of the uranium isotopic composition in the material that is usually in the form of particles distributed on cloth wipes.

Secondary ion mass spectrometry (SIMS) is an effective isotopic measurement method for this purpose because of its ease of sample preparation, sensitivity, and capability to locate uranium-bearing particles among background debris in an automated search mode. NIST has played a significant role in developing and testing these methods, and in transferring this capability to the IAEA Safeguards Analytical Laboratory in Austria.

One limitation of SIMS is the existence of mass spectral interferences that are combinations of atoms of different elements forming an ion with the same nominal mass as an isotope of interest. NIST recently acquired a SIMS instrument that offers the possibility of distinguishing an isotope of interest from a potentially interfering species through improved mass spectral resolution. The purpose of this study was to define the instrumental conditions to achieve this separation while minimizing the effect on ion transmission. An instrument and a set of procedures that can realize these results will benefit organizations associated with nuclear forensics through increased reliability of uranium isotopic data.

**Major Accomplishments:** A series of measurements of the uranium mass spectral peak shape from a uranium oxide isotopic reference material were made at different combinations of entrance and exit slit settings that control the mass resolving power and peak shape, but also affect the secondary ion transmission. The results of some of these measurements are shown in Table 1 and Figure 1. The conditions of the first row correspond to 100 % transmission of uranium ions through the mass spectrometer, the conditions of successive rows correspond to narrower peak shapes, but with some reduction in ion transmission.

Reliable isotopic abundance measurements require that potential mass spectral interferences should make an insignificant contribution. A calculation of the exact masses of all possible ion combinations shows that lead-containing molecular ions are the most closely spaced potential interferences to the uranium isotopes at  $m/z$  234, 235, 236, and 238. An example is the  $^{208}\text{Pb}^{27}\text{Al}$  ion that would be centered 0.08575 mass units below the  $^{235}\text{U}$  mass position. To demonstrate the degree of rejection of this peak, should it occur, the  $^{235}\text{U}$  peak shapes were used to simulate PbAl at its mass position so the contribution of the interfering peak tail at the  $^{235}\text{U}$  mass position could be calculated. This procedure is shown graphically in Figure 1 and numerically in the last column of Table 1. The conclusion from these studies is that a rejection of this worst-case

spectral interference by a factor of  $10^5$  can be achieved with an insignificant reduction in ion transmission by appropriate instrumental settings.

**Future Plans:** Additional studies of uranium ionization efficiency and isotopic measurement protocols are expected to further improve the measurement of uranium isotopic composition in small particles by SIMS.

| <i>Slits<br/>(<math>\mu\text{m}</math>)</i> | <i>Relative<br/>Transmission</i> | <i>MRP<br/>@ 10 %</i> | <i>Rel. Tail Sig.<br/>@ <math>^{235}\text{U}</math></i> |
|---|----------------------------------|-----------------------|---|
| 588/350                                     | 1.00                             | 2520                  | $8.8 \times 10^{-5}$                                    |
| 250/350                                     | 0.98                             | 2540                  | $1.2 \times 10^{-5}$                                    |
| 180/350                                     | 0.85                             | 2600                  | $< 1.0 \times 10^{-5}$                                  |
| 150/300                                     | 0.76                             | 3080                  | $< 1.0 \times 10^{-5}$                                  |

Table 1. Relative ion transmission and mass resolving power for  $^{235}\text{U}$  peak at various entrance/exit slit settings. Last column is relative contribution of peak tail at  $^{235}\text{U}$  mass position if peak is shifted to  $^{208}\text{Pb}^{27}\text{Al}$  mass position to simulate mass spectral interference.

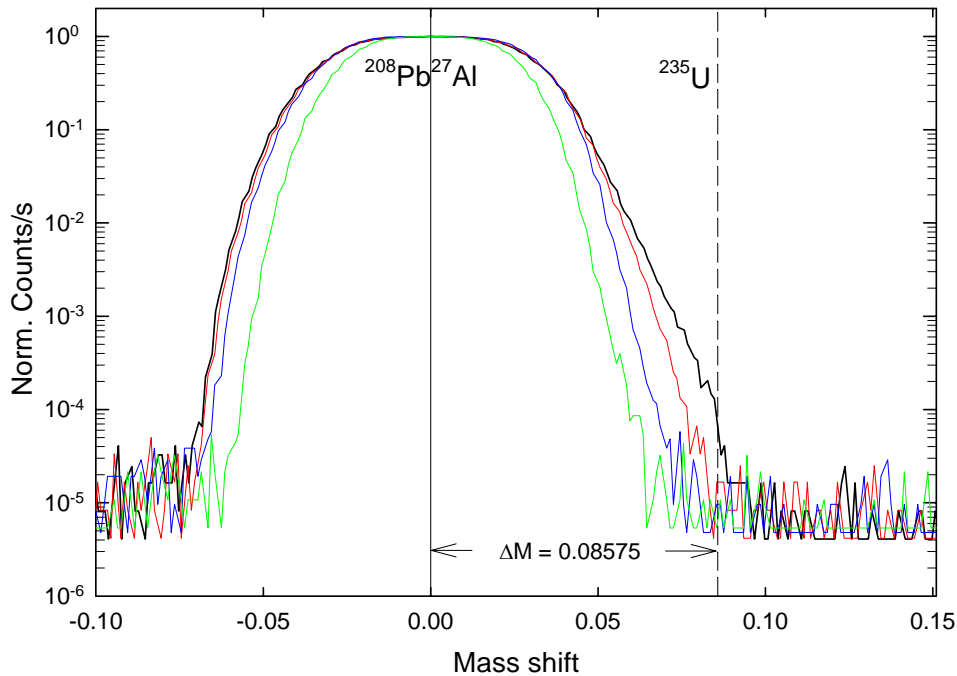


Figure 1. Peak shapes of  $^{235}\text{U}$  for slit settings shown in Table 1, shifted to mass position of  $^{208}\text{Pb}^{27}\text{Al}$  to show peak tail contribution at  $^{235}\text{U}$  mass position. The black, red, blue, and green traces correspond to the slit settings of rows 1-4 in Table 1, respectively.

## **Highlight Title Quantitative Analysis with the TES Microcalorimeter**

**Authors** – Terrence Jach, Nicholas Ritchie, Joel Ullom (Div. 817, Boulder), James Beall (Div. 817, Boulder).

Identify Program Chem and Instru

### **Context and Approach:**

Quantitative analysis is at the heart of much of chemistry and materials science. On the microscopic scale, quantitative analysis with an electron microscope or microbeam probe has become the standard technique in universities and industry. It has, for example, played a key role in the development of our electronics industry. The standard techniques for analysis of characteristic x-rays produced by the beam of an electron microscope are the energy dispersive (ED) methods (represented by the lithium-drifted silicon detector and silicon drift detectors) and the wavelength dispersive (WD) methods (detectors based on x-ray diffraction). ED methods cover a wide energy range but have poor resolution, while WD methods have high resolution over a narrow energy range.

The Transition Edge Sensor (TES) Microcalorimeter invented at NIST is a relatively new method of detection that embodies the best characteristics of each. The detector is capable of high resolution over a broad energy range. It incorporates a small x-ray absorber cooled to very low temperatures (<100 mK) and a thermometer capable of measuring the temperature rise from the absorption of single x-ray photons. The thermometer, a thin film of metal maintained at its superconducting transition, is capable of a remarkably linear response that makes it ideal for the energy resolution of characteristic x-rays from nearly all chemical elements.

While the detector was initially subject to the kind of problems typical of a new and sensitive measurement technology, we have overcome the most troublesome issues and have proceeded this year to prove the detector's value in scientific applications. In cooperation with Joel Ullom and James Beall of the Quantum Electrical Metrology Division (817, Boulder) we have undertaken a program that demonstrates the ability of the detector to conduct quantitative analysis in situations that would have been previously impossible.

### **Major Accomplishment(s)**

This year we demonstrated for the first time: 1) quantitative analyses on non-stoichiometric NIST Standard Reference Materials which measured the accuracy of the microcal detector, and 2) the observation of x-ray emission from a chemical compound with sufficient resolution to identify its valence band.

The microanalysis of elements with an electron probe is a primary goal of the TES Microcalorimeter program. The microcalorimeter detector has been incorporated into a dedicated JEOL 840 electron microprobe for this purpose. This year we conducted several sets of measurements on NIST SRM glasses (K411 and K458) to compare the accuracy of Microcalorimeter measurements with the chemical assays which certify these SRM's.

Our quantitative analysis results covered the elements Ba, Ca, Fe, Mg, O, Si, and Zn over an energy range of 500 eV—8000 eV. Characteristic x-ray line intensities of K and L transitions were measured in spectra from standard compounds and from the materials to be analyzed. In both, we included lines from the above elements which lie so close together in energy as to interfere with each other. The excellent energy resolution, combined with the broad energy range, allowed us to carry out an analysis of element concentrations that would be impossible to obtain by single spectra from conventional detectors. The

overall discrepancies—1% in total concentration, and a maximum of 8% in relative concentration of a weak element—are quite acceptable for many analyses. The first figure below illustrates a spectrum obtained in 1000 s of live counting time.

We also obtained an x-ray fluorescence spectrum from a compound which demonstrates chemical specificity. As a test case, we selected the chemical compound BN in which the excited state of a N 1s core hole is directly filled with valence electrons—2s and 2p electrons from the N atom, as well as with valence electrons from other atoms in the compound. The hybridization of these atomic states into molecular orbitals results in a valence electron density of states that extends over approximately 30 eV and which is specific to this compound. The resulting emission spectrum extends over a similar energy width. We compared the x-ray emission spectrum by the Microcalorimeter with a high-resolution spectrum that we obtained on a grating spectrometer beamline at the Advanced Light Source at Lawrence Berkeley Laboratory. A comparison between the TES Microcalorimeter spectrum and the light source spectrum broadened to the same 4 eV resolution, shown in the second figure, illustrates that we are obtaining accurate evidence of the valence band.

**Impact** – NIST has been working with a small company (a recipient of ATP funding) to produce a commercial realization of the TES Microcalorimeter detector. This is the sole US effort to compete with comparable efforts in Europe and Japan. Several presentations that we gave during the year have aroused considerable interest and inquiry into the availability of the detector. The response to our results was so strong that NASA has invited us to participate in a study on the feasibility of TES Microcalorimeter incorporation into the lunar exploration program.

**Future Plans** –This activity has a broad future ahead of it. The program of quantitative analysis will continue to determine the limits of its applicability during the current fiscal year. The program to obtain high resolution valence band x-ray emission spectra for chemical analysis will be augmented by the design and construction of a new detector which will cover an energy range of about 1 keV with 1 eV resolution.

**Publications, Patents** –

“Quantitative Analysis with the Transition Edge Sensor Microcalorimeter X-ray Detector,” Terrence Jach, Nicholas Ritchie, Joel Ullom, and James A. Beall, *Advances in X-ray Analysis*, Submitted.

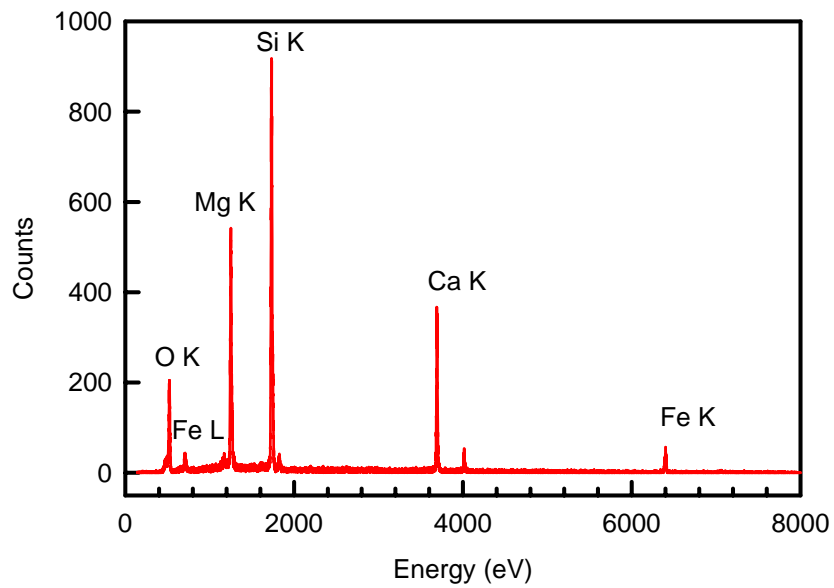


Fig. 1 Spectrum of K411 glass, 1000 s live time.

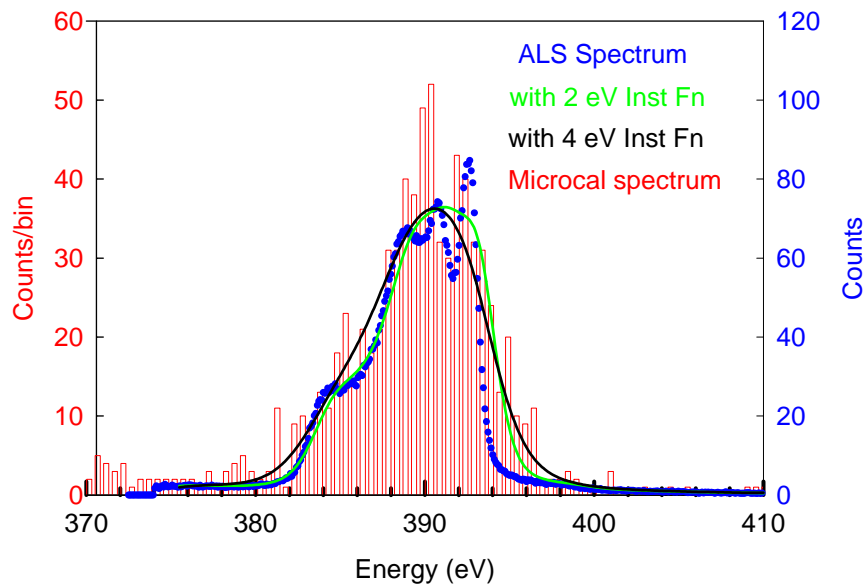


Fig. 2 Valence band x-ray emission spectrum of BN from the microcalorimeter and from beamline 8.0.1 of the Advanced Light Source, broadened to 2 eV and 4 eV resolution.

**Title:** Electron Probe Quantitative Analysis of Carbon and Nitrogen in TiC and VN Films.

**Authors:** Ryna Marinenko and Scott Wight

**Purpose:** In FY06 the Surface & Microanalysis Science Division was invited to participate in an informal measurement round-robin exercise on the concentration of carbon and nitrogen, two low atomic number elements that are difficult to analyze with the electron microprobe. The project which was conducted by CCQM (Consultative Committee on Quantitative Measurements) a committee of the BIPM (Bureau International des Poids et Mesures) included primarily national laboratories. The three samples to be measured were two films (2  $\mu\text{m}$  to 3  $\mu\text{m}$  thick) of Vanadium-Nitride and Titanium-Carbide and a bulk steel containing carbon. The goals of this project were not only to provide CCQM with the data for their round robin, but also to develop new analytical protocols and standards to improve our ability to analyze light elements.

**Major Accomplishments:** CCQM provided the two specimens of 2  $\mu\text{m}$  to 3  $\mu\text{m}$  thick films of TiC and VN on stainless steel. The analysis technique, experimental parameters, and quantification data reduction procedures were optional. We chose to use wavelength dispersive electron probe microanalysis (WDS-EPMA). The other seven laboratories used EPMA with the exception of one that used X-ray photoelectron spectroscopy (XPS). C and N are difficult to analyze by EPMA for several reasons: 1) the  $K\alpha$  x-rays of both elements are readily absorbed by the matrix, especially by heavier elements; 2) the x-ray spectral peaks for both C and N are broad and shift with the bonding environment of the element; 3) stoichiometric reference standards are not readily available.

The most difficult aspect of this project was the search for and characterization of reference standards for the analysis. Fortunately, we were able to obtain three TiC specimens as well as a commercial powder of VN that had particles in the 8  $\mu\text{m}$  to 10  $\mu\text{m}$  diameter range, large enough for analysis with the electron probe without sampling areas outside of the particles. We tested these specimens for microheterogeneity and quantified them with pure elemental Ti and V standards. We determined that one of the TiC specimens, a single-crystal, and the VC particle specimen was stoichiometric. This was fortunate since TiC has a complex phase diagram and often occurs in a substoichiometric form with vacancies in the sublattice

Having reference standards similar to the films being analyzed enabled us to use peak height measurements for quantification as no peak shifts between the standard and unknown were observed. The films were thick enough to be treated as bulk specimens (confirmed by consistencies in our data and by Monte Carlo calculations) and were analyzed at multiple excitation potentials, 7.5 keV, 10 keV, 12.5 keV, and 15 keV, all at a current of 50 nA. We used synthetic multilayered crystals, LDEC for C and OV080 for N. For Ti and V we used a PET crystal. Fifty points were analyzed for each film. Our results from the four voltages had an uncertainty (a single standard deviation) of 1 % relative for both C and N. A small uncertainty between the results of the different voltages is used to validate the data reduction procedure which corrects for other elements present in the matrix. Our data reduction software, Probe for Windows (PFW) can test binary compound data using all available correction procedures with as many as

five different mass absorption coefficient tables to determine which combinations are the most accurate. With this help we chose the Armstrong/Love-Scott with LINEMU MACs to quantify the raw data for the quantification of both the reference standards and the films.

In table 1 our results are compared to the range of values reported in the first round of reported by CCQM. The range of values probably reflects the differences in excitation potentials, data collection and processing. Our results for C in TiC are at the lower end of the range but there are four other laboratories' results, including the one using XPS with values only 1% to 2 % mass fraction higher than the NIST result. This low value for C in TiC also reflects the fact that there is no mass balance for us and the four other laboratories. Some of the other participating laboratories may not know this since the initial request was to analyze for C only. After these first results were reported from CCQM, all laboratories were requested reanalyze for the cations as well using the same voltage.

Our results for N in VN are within 1 to 2 % mass fraction of three other laboratories again including the XPS result. The mass fraction balance is not as serious in this sample, but we noted the presence of Ar in an energy dispersive spectrum and the presence of what may be small impurities although CCQM claims that they are not present.

**Future Plans:** We plan to continue working with CCQM on this project as needed. It has demonstrated the difficulty of achieving agreement between laboratories in the quantitative analysis of light elements, so we expect additional instructions will be forthcoming.

**Pubs/Outputs:**

1. Two reports in spreadsheet form, one each for TiC and VN with worksheets of data at each kV sent to John Nunn, NPL with attached comments.
2. Abstract and poster - Marinenko, R., *An Approach to the Evaluation of Titanium Carbide Specimens for Microanalysis Standards*, Proc. Micros. & Microanal.Mtg. 2006, Chicago, Ill, Micros. & Microanal., **12**, Suppl. 2, Kotula, P. et. al., eds., Cambridge U. Press, Cambridge, UK, 876CD.

| Composition in % Mass Fraction (Rel 1 $\sigma$ Uncertainty in % in Parentheses) |            |            |       |            |            |       |
|---|------------|------------|-------|------------|------------|-------|
|   | Ti in TiC  | C in TiC   | Total | V in VN    | N in VN    | Total |
| NIST Avg.   | 68.76(2.1) | 21.98(2.5) | 90.74 | 78.46(1.9) | 19.57(3.5) | 98.63 |
| CCQM Range  |            | 21.98-32.8 |       |            | 15.3-26.4  |       |
| Nominal Comp.   | 79.95      | 20.05      |       | 78.43      | 21.57      |       |

## **Title: Fitting of Auger Electron and Secondary Electron Line Scans with the Extended Logistic Function.**

**Authors:** Scott A. Wight and Cedric J. Powell

### **Purpose:**

Auger-electron spectroscopy (AES) is used for surface analysis and for determining variations of composition from one phase to another in an inhomogeneous specimen. A common application of AES has been the determination of composition as a function of depth in thin-film specimens by sputter-depth profiling. Additionally, the scanning Auger microscope (SAM) is also used to analyze heterogeneous samples with line scans which are the measurement of chemical composition along a line on the sample surface.

Kirchhoff, Chambers and Fine [J. Vac. Sci. Technol. A **4**, 1666 (1986)] proposed the use of an extended form of the logistic function to describe compositional changes between two materials as a function of depth from an AES sputter-depth profile. This approach was found to be a convenient means of objectively determining parameters describing the interface width and possible asymmetry of the profile.

We have expanded upon this work by applying the logistic function to line profiles of both secondary electrons and Auger electrons. Where this may have its greatest impact is in the measurement of instrumental resolution. Currently, secondary electron imaging of gold islands on carbon is the standard test for secondary-electron imaging resolution in electron microscopes. The Au-island images are routinely indexed manually to determine the instrument resolution. With the higher resolution of today's electron microscopes, the manual determination of the resolution relies upon a subjective selection of the edges of the gold particle to determine if an instrument is operating within specification. Unlike manual fitting, the logistic function provides objective measures of the position, width and possible asymmetry of an interface.

### **Major Accomplishments:**

We fitted Auger-electron (AE) and secondary-electron (SE) line scans from two types of specimens with the logistic function. The fits for a gold island on a carbon substrate provided useful measures of lateral resolution in our SAM (values between 22 nm and 34 nm compared to a specification of 19 nm at these conditions) and showed clear evidence of "tails" associated with imperfect alignment (Figure 1). An analyst might wish to minimize the magnitude and range of these tails while aligning a SAM to maximize beam current and minimize the beam width. We also used the logistic function to fit SE intensities of a fractured Ni/Cr multilayer sample and SE and AE linescans across a sputtered crater of this sample (Figure 2). The fits using the logistic function gave useful measures of the interface width (the average value is 23.3  $\mu\text{m}$ ).

### **Future Plans:**

A software implementation of the logistic function is being developed by William Kirchhoff in our Division. This Windows-compatible software, currently in a beta test phase, will conveniently estimate the position, width and asymmetry of an interface

between two dissimilar materials. This software will be disseminated through the Surface and Microanalysis Science Division [web page](#).

**Pubs/Outputs:**

SA Wight and CJ Powell “Evaluation of the shapes of Auger- and secondary-electron line scans across interfaces with the logistic function” Journal of Vacuum Science and Technology A, 24(4), 1024, Jul/Aug 2006.

**Figures:**

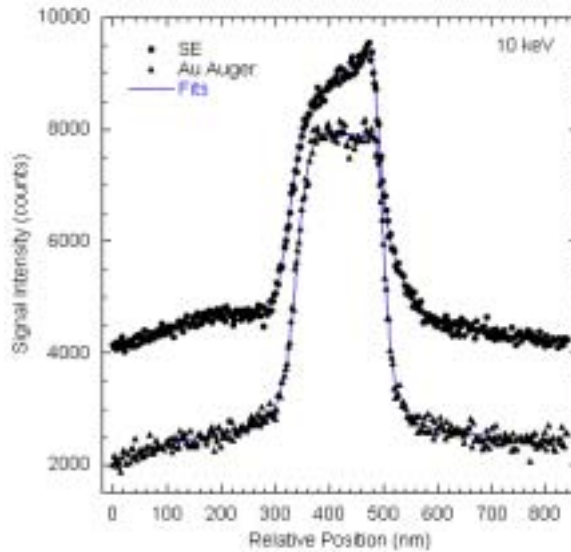


Figure 1: Example fits with the logistic function to secondary electron and Auger-electron line scans across a gold island measured with primary beam energy of 10 keV.

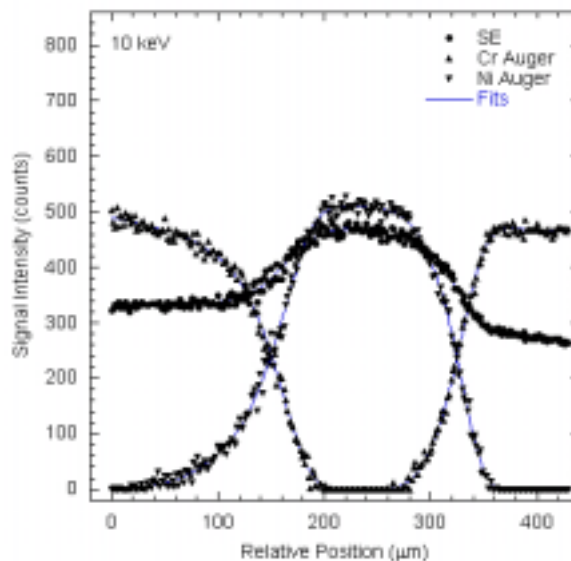


Figure 2: Fits with the logistic function to Ni and Cr Auger-electron and secondary-electron line scans across an edge of a sputter crater of a Ni/Cr multilayer measured with a primary beam energy of 10 keV.